The Thesis Committee for Sebastian Calvache Mejia
certifies that this is the approved version of the following thesis:

Development of a Multiphase Flow Simulator For Drilling Applications

Committee:

Kamy Sepehrnoori, Supervisor

Paulo Roberto Ribeiro

Development of a Multiphase Flow Simulator For Drilling Applications

by

Sebastian Calvache Mejia,

Thesis

Presented to the Faculty of the Graduate School of

The University of Texas at Austin

in Partial Fulfillment

of the Requirements

for the Degree of

Master of Science in Engineering

The University of Texas at Austin

August 2017

To my Parents, for their unconditional love and support in my endeavours.

Thank You.

Acknowledgments

First, I would like to express my sincere gratitude and appreciation to my supervisor, Dr. Kamy Sepehrnoori for his support throughout the duration of my time at The University of Texas. I will forever cherish his mentorship, guidance and patience. I would also like to thank Dr. Paulo Ribeiro for taking the time to read through my thesis and helping me with any queries I had. His attentiveness and feedback helped me immensely.

Second, I would also like to thank Mahdy Shirdel for taking the time to help me understand UTWELL. Both Claudio Loiola and Felipe Lucio for their support in helping me with any queries I had concerning the modelling of the gas kick stages.

Third, I'd like to thank my officemates for all the fun times that we had in the office, helping make it a great environment to work in. Special thanks to Mehran Mehrabi for guiding me as I slowly built the simulator and to Bruno Fernandes for helping me with any coding related difficulty.

I'd like to thank Denise Candelo, for her love and support; thanks for always being there for me. My friends, Nithin Aikkarayil, Ben Ayton, Kevin Tati, Liz Butcher, and others not mentioned implicitly who constantly provided me with support and encouragement.

My parents, Jorge and Lucila, for always supporting my decisions and being my biggest sources of inspiration. My grandmother, for her constant support and love. My uncles, aunts, and cousins, whom always provided encouragement.

Lastly, God, for blessing me with this opportunity.

Sebastian Calvache Mejia

The University of Texas at Austin

August 2017

Development of a Multiphase Flow Simulator For Drilling Applications

Sebastian Calvache Mejia, M.S.E
The University of Texas at Austin, 2017

Supervisor: Kamy Sepehrnoori

Drilling, or gas kick, simulators are becoming prevalent in industry due to their ability to replicate wellbore conditions that are not feasible in a laboratory setting. This is becoming more desirable as deeper wells are being explored. One of the biggest dangers that could happen during drilling operations is the onset of a gas kick. This occurs when a zone in the formation whose pressure is higher than that of the wellbore is breached. This allows for the undesired influx of formation fluids into the wellbore. If left uncontrolled, it could develop into a blowout.

Gas kick simulators allow for testing of procedures that could be used to contain kicks at such depths. Furthermore, the use of drilling simulators could provide more insight into other phenomena. These include wellbore breathing and fracture ballooning, that cause similar kick symptoms at the surface and lead to expensive misdiagnosis, and the dissolution of gas into oil based mud, which could delay the identification of a kick. This thesis investigates the development of the initial integration of a drilling simulator into UTWELL, the wellbore simulator program developed at The University of Texas at Austin, by implementing a gas kick module.

The transport equations of mass and momentum conservation were discretized using a Semi-Implicit Homogeneous Method over a one dimensional staggered grid. The multiphase phenomena were modelled using a Drift Flux approach as opposed to a mechanistic, Two Fluid approach. This was due to increased stability of the solution and faster computation time, despite the risk of loosing accuracy.

The simulator was successful at simulating single phase flows for fluids with distinct rheology models, and with wellbores with discontinuities in the geometry. When attempting to simulate the well control of a gas kick in water based mud, the results were mixed. Attempt at simulating a 'Floating Mud Cap' method failed due to the simulator's inability to perform drainage functions that allow for the raising and lowering of the mud level in the wellbore. However, the simulator was successful at capturing the behaviour of the gas kick as it entered and migrated through the wellbore, matching literature results.

The simulator was compared to experimental data gathered from a test well. Three different scenarios were tested: No Drillstring, Semi-Submerged Drillstring and Drillstring at the Bottom. In all three cases, there was a good match between the experimental and simulation results for the bottomhole and choke pressures. The pit gain was severely overestimated in the 'No Drillstring' and 'Semi-Submerged Drillstring Case', however this was due to a higher influx of simulated gas having entered the wellbore during simulations. The 'Drillstring at the Bottom' simulation matched well with all data and with other simulators.

Recommendations included full integration and testing of a compositional model to simulate oil based mud cases, implementation of automatic choke control and special flux splitting techniques in the discretization in order to better handle pressure waves caused by discontinuities.

Contents

List of Tables

List of Figures

Chapter 1

Introduction

The handling of gas kicks during drilling operation is one of the most prevalent and persistent problems faced by industry. Improper handling of the gas kick can lead to blowouts, the uncontrolled flow of hydrocarbons to the surface, which can lead to the destruction of equipment, environmental damage, and possible loss of human life. Drilling, or gas kick simulators, have been developed in order to gain a better understanding of the phenomenon. By using drilling simulators, engineers can not only predict how a kick could behave under specific drilling conditions, but test out a variety of well control methods in order to determine the safest and most effective course of action to safely remove the kick from the wellbore.

A gas kick occurs when the pressure of the formation (or reservoir) is higher than the pressure inside the wellbore. The resulting pressure gradient allows for the influx of formation fluids into the wellbore. The entering fluids thus begin to displace the drilling mud initially present inside the wellbore. Since formation fluids, gas, oil or water, tend to be less dense than drilling mud, this causes for the pressure inside the wellbore to decrease. This leads to a bigger pressure gradient between the formation and wellbore, and consequently, a higher influx of formation fluid. If left uncontrolled, the large influx could lead to a blowout.

In the wellbore, the pressure at the bottom-hole is primarily controlled through the use of drilling mud, with the Bottom-Hole Pressure (BHP) being a function of the hydrostatic liquid column and frictional pressure losses during circulation. During drilling

operations, the BHP is monitored to ensure it is kept at a higher pressure than that of the formation in order to prevent a kick from ocurring. In the event a kick does occur, one of the primary warnings is an increase in the outflow of mud as it is displaced by the entering formation fluids. Once the gas kick is verified, various well control methods can be employed to regain control of the well.

The majority of well control methods are based on the concept of first increasing the bottom hole pressure until it is higher than the formation pressure in order to stop the influx of fluid. Subsequently, new mud is circulated in order to flush the kick in a safe manner. Classical well control methods include the Drillers Method and the Wait and Weight Method. In both methods, the kick is handled by pumping a new, higher density mud, referred to as kill mud, allowing for the establishment of a BHP higher than the kick pressure. The two methods differ in that the Wait and Weight Method requires only one circulation cycle to flush out the kick whereas the Drillers Method requires two circulation cycles. A third classical method is that of Bullheading where the kick fluids are forcibly pumped back into the formation. Due to the high risk of fracturing the formation, this is only employed when toxic hydrogen sulfide is present in order to prevent it from reaching the surface.

Newer well control methods include Managed Pressure Drilling (MPD) strategies. In these methods, a control system is implemented into the wellbore where the bottomhole pressure is controlled by modifying the annular backpressure at the surface, allowing for the BHP to be increased or decreased as the operator sees fit. This can be done via the use of a choke, by changing the height of the hydrostatic column, etc. These newer methods provide a faster response time than the classical methods since they do not require for a heavier drilling mud to be pumped, leading to improved drilling efficiency, economic benefits and safety.

This thesis chronicles the integration of a gas kick simulation model into UTWELL, the wellbore simulator program developed at The University of Texas at Austin. The main focus of this thesis will be to set up the basic foundations of the program and compare the code with experimental data to study its robustness and effectiveness at simulating real

scenarios and MPD strategies.

1.1 Importance of Topic

Well control procedures to control gas kicks have been continuously developed and improved upon over the past century to increase efficiency and safety. Furthermore, since multiphase simulators are heavily dependent on empirical correlations and models, and the nature of multiphase flow is highly chaotic, expecting a simulator to perfectly predict the behavior of a gas kick is unreasonable. Thus, the long term objective of developing a gas kick simulator is not to simply simulate the behavior of the gas kick within the wellbore accurately, or determine how to best circulate out of the well. Instead, the objective is to develop a tool that would allow for the study of phenomena related to gas kicks, and other drilling procedures, that would otherwise be difficult to measure in a laboratory environment. This is due to difficulty in setting up experiments with similar ambient conditions as those seen in wellbores. This is becoming more prevalent due to the deeper environments which are now being drilled to.

There are various phenomena which occur inside the wellbore during drilling operations that are yet to be fully understood. These include, but not limited to, fracture ballooning and wellbore breathing which could lead to the misdiagnosis of a gas kick. These events, which could occur during tripping operations, cause for the outflux of mud from the wellbore due to elasticity effects in the rock formation (Mehrabi, Zeyghami, and M. Shahri (2012) and M. P. Shahri and Mehrabi (2012)). The transient flows caused by these phenomena at the outlet of the wellbore is expected to be somewhat different than those seen during the event of a gas kick. Hence, the development of a robust transient gas kick simulator could help in identifying the characteristic features of such flows and lead to reduction in nonproductive time (NPT) and consequently economic savings.

Another phenomenon frequently experienced but hard to study is the effect of cuttings at the bottomhole. Cuttings occur due to residue of the formation that is too heavy to be transported by the drilling mud and hence settles at the bottom of the wellbore. Deposition of cuttings into the wellbore lead to pressure loss and circulation issues, which

could result in fracturing the formation and subsequent economic losses. A robust drilling simulator would allow us to be able to study how cuttings congregate at the bottomhole and what could be done to circulate them in an efficient manner.

Furthermore, there has been little development in the field of multiphase flow correlations concerning Non Newtonian fluids. Since the majority of drilling muds, particularly oil based drilling muds, exhibit non Newtonian behavior, development of a robust drilling simulator for industrial application could stimulate advancements in this field.

1.2 Scope and Objectives

Due to the large scope that the development of a fully functional drilling simulator could entail, the primary scope of the project will be defined. The objective will be to organize UTWELL so it can handle simple kick cases and produce results that adequately match literature and experimental results.

This will be done by thoroughly testing the simulator with a multitude of cases. First, the simulator will be tested to see if it can match analytical solutions for single-phase flow. Second, the multiphase flow function of the simulator will be tested by seeing if it can match results produced by other recent simulators. Lastly, the simulator will be tested with field data taken from the Marques (2004) and Avelar (2008) studies to test whether it is robust enough to replicate experimental data.

One of the main aspects of the simulator that will be tested is that of managing a choke valve at the outlet in order to induce the backpressure required to keep the well above the kick pressure. In this thesis, this will be done through a trial and error approach where the user will have to change the boundary conditions in each run through an iterative approach, however research has been done in the control systems and algorithms required in order to make such a function automatic (Ambrus et al. (2015)).

1.3 Organization of Chapters

The following paragraphs give a brief overview of the contents of each of the chapters in this Thesis.

Chapter 2 presents a literature review on the recent development of gas kick simulators and multiphase flow.

Chapter 3 presents background information on the mathematical equations that describe the physical phenomena associated with multiphase flow. It also includes details on the correlations and models used in the UTWELL simulator and the modelling of the different stages present in the control of a gas kick.

Chapter 4 provides an introduction to the UTWELL code, detailing the discretization and solution algorithm used to solve the transport equations described in Chapter 3.

Chapter 5 presents the simulation results, and analysis, for the various tests employed to examine the robustness of UTWELL for gas kick simulation.

Chapter 6 states the final conclusions of this project along with ideas for future work and the consequent steps that should be taken to improve upon the simulator.

Chapter 2

Literature Review

In the following section the significant advancements that have been made in the development of gas kick simulators and associated fields are reviewed.

2.1 Gas Kick Simulators

The development of gas kick simulators begun almost 50 years ago, with Leblanc and Lewis (1968) first analyzing the effects of annular backpressure on controlled gas kicks. In their analysis, a two phase, frictionless, immiscible flow was assumed since only the recirculation stage of the kick was considered. Their argument being that only small flow rates are typically used in recirculation processes. The gas bubble was modelled as a discrete region travelling at the same velocity as the mud and occupied the whole cross sectional area. Furthermore, their solutions were based on analytical solutions as opposed to discretized numerical models. Despite only focusing on the well control stage of the gas kick and being simplistic, their work is considered the first mathematical model for gas kick behavior.

Nickens (1987) developed a simulator that could handle wells with variable geometries as well as non Newtonian models for the liquid phase. Attempting to demonstrate the transient effects that occur during a kick, he opted to use a discretized numerical approach as opposed to analytical equations. He was also one of the first to couple the wellbore with a gas reservoir by using a radial flow boundary condition, hence making the entry of gas dependent on the bottomhole pressure as opposed to injecting a controlled volume of gas. Throughout his work, he stresses the importance of incorporating robust correla-

tions and models to represent the different physical phenomena. To illustrate, he simulates the same case using two different multiphase models, that of a single bubble compared to distributed gas. His results highlighted the discrepancies caused by the two models, with the single bubble model producing higher casing shoe pressures and requiring more mud to be pumped to recirculate the kick out of the well. Despite highlighting the importance of selecting adequate correlations, and the simulations showing the expected pressure trends during circulation, Nickens work did not include experimental or field data to verify which model better described reality.

The first attempt at a gas kick, and wellbore model, simulator at The University of Texas at Austin was by Starrett, Hill, and Sepehrnoori (1990). In their work, they model a horizontal diverter attached to the top of the wellbore in order to monitor the effects caused by the kick. Similar to Nickens, Starret et al. employed a sensitivity analysis in order to study the effects the diverter had on the kick, modifying both the length and the radius of the diverter. Throughout the simulation, the pressure at the outlet was kept at atmospheric conditions (no shut in is simulated). Furthermore, the simulator was not compared to either experimental or field data, hence not testing for accuracy of the results produced. It wouldn't be until the work of Pourafshary (2007) and Shirdel (2013) that work on a wellbore/multiphase simulator would be revisited at UT Austin.

Other significant wellbore simulator attempts include the work of Santos (1991) who studied the case a gas kick occurring in a horizontal wellbore. In his study he identifies three key regions of analysis: single-phase region where the displacing fluid flows behind the gas bubble at steady state conditions, a two-phase region where the multiphase region flows in unsteady state conditions, and a single-phase zone where the drilling fluid is ahead of the gas bubble and is being accelerated by gas expansion. The paper was one of the first to consider inclined/deviated wells and also analyses the pressure effects of swabbing during drilling operations. Additional work on the study of deviated wells is accredited to Rommetveit and Vefring (1991) who compared their RF Kick simulator to field data for a 60°deviated well. Furthermore, they consider the problems surrounding oil based muds with kicks and attempt to model the effect of solubility by using Argon/Nitrogen mixture as the composition of their gas. In their normalized results, the simulator seemed to agree

with the general trends of the data, however was constantly over predicting the bottomhole pressure of the well. They also demonstrate how fine tuning and careful selection of the gas rise velocity parameters is critical for simulating the gas kick, else important well control parameters will be incorrectly determined.

Nunes, Bannwart, and Ribeiro (2002) provided a mathematical model for modelling a gas kick in deep underwater scenario. In their work, they employ an iterative analytical approach to determine the effects of water depth, pump flow, pit gain and mud density on the choke pressure. The works of Avelar (2008) and Loiola (2015) expand upon the work of Nunes by opting for a discretized numerical approach as opposed to analytical. In their work, they compare the results of their respective simulators with the experimental results provided by Marques (2004) who performed a series of well control methods on a test well. Avelar (2008) presents a two phase model to show the robustness of the simulator whereas Loiola (2015) expands upon this work by incorporating a three phase compositional model. In both cases, the simulators provided good agreement with the test data. Avelar, Ribeiro, and Sepehrnoori (2009) extend the work by examining the effects of the water depth on the BHP, choke pressure, pit gain and outlet flow rate on a hypothetical test well. Furthermore, Loiola (2015) studies the effects of using oil based mud compared to water based mud. His results mirror that of to Rommetveit, as the gas kick took longer to be identified in the oil based mud because of increased solubility.

Additional related topics include the work of Fjelde and Karlsen (2002) and Udegbunam et al. (2015), who focus extensively on the propagation and movement of pressure waves in tubes, and their applicability for oil and gas systems. In both works, they apply higher order Computer Fluid Dynamics (CFD) discretization methods in order to better handle the transfer of mass and momentum between adjacent nodes. In Fjelde and Karlsen (2002), they demonstrate the use of high resolution hybrid primitive-conservative upwind schemes to capture the movement of pressure waves in a shock tube with two phase flow. They first confirm the accuracy of their simulator by presenting various shock tubes and comparing with analytical solutions. Consequently, they expand their set of results to measure the propagation of pressure waves along horizontal and vertical pipelines. In Udegbunam et al. (2015), also supervised by Fjelde, they apply the simulator for under bal-

anced drilling (UBD) and managed pressure drilling (MPD) cases, however they simplify the simulation by assuming constant drift-flux parameters and the same frictional loss correlation for liquid and gas phases. In this work, they analyse the effect that choke pressure, kick volume, and grid size have on solutions. One of the main conclusions was the heavy dependence of mesh size on the converged solution.

Recent work that has focused on the well control system as opposed to wellbore modelling is that of Ambrus et al. (2015). Focus is shifted towards the control system used to stabilize the bottomhole pressure of the well during the kick for automated well control applications. Ambrus uses a simplified, explicit transient model in order to measure bottomhole pressure as a function of the choke behavior. Simulator results were compared to a commercial simulator with good agreement between the results, highlighting its potential use in a more robust system.

2.2 Multiphase Flow Modelling for Gas Kick Applications

Due to the simplifications made by Leblanc and Lewis (1968) in their original work, large discrepancies were found between the computer calculated annular profile and field data. The reason for this was attributed to gas-slip velocity phenomena as well as frictional pressure forces. Rader, Bourgoyne Jr, and Ward (1975) would follow up on their work by studying the factors affecting the bubble rise velocity of Gas Kicks. These included appreciation of the pipe geometry, variation in density, holdup and gas expansion. Their work was essential in order to implement gas-slip correlations in mathematical backpressure models, hence being the first in depth analysis of the multiphase flow mechanics involved in gas kicks.

The effects of slippage between phases, considered one of the more sensitive and critical parameters as illustrated by Nickens (1987) and Rommetveit and Vefring (1991), has been the focus of extensive research. In order to take account for the effects of slippage, methods such as the Drift Flux Method (Mishima and Ishii, 1984) have been developed to provide a simple method where the effects of slip are dependent on the holdup of the phases. In this method, the mixture velocity is used in order to determine the respective gas and liquid velocities depending on the multiphase flow regime. Similar to how single-phase flow

is separated between laminar and turbulent flows, various types of multiphase flow can be grouped in distinct flow categories which include bubbly, dispersed, slug, annular and mist flows (Taitel and Dukler, 1980). Research has focused on the development of correlations that will give the appropriate definition of the drift flux parameters for a given flow regime. Recognised contributions include the works of Nickens (1987), Hibiki and Ishii (2003) and Shi et al. (2005).

The advantages of the drift flux model include their fast calculation times and being simple to implement, along with being capable of being continuous and differentiable. However, they do not fully take into account momentum transfer between the phases and are not ideal for flows with high density and viscosity contrasts. Furthermore, certain correlations may only be acceptable within certain criterion, requiring tuning of parameters in order to correctly simulate the desired physical phenomena.

More complicated models, such as the Two Fluid Model, have also been studied in detail. In these methods, slippage between phases is accounted for by calculating the shear stresses different phases exert on each other during flow. Since these methods are based on the transport equations, with each phase requiring a set of mass, momentum and closure equations, they can provide more accurate results than the drift flux approach over a wider range of velocities (Yuan and Zhou, 2009). However, these methods are harder to implement since the related closure equations are heavily dependent on different parameters for the distinct flow regimes, hence leading to discontinuities. The presence of discontinuities, as well as the hyperbolic nature of the transport equations, are a source of system instability regardless of the solution methods and has been an extensive research field according to Shirdel (2013).

Parallel to the development of slip flow correlations was also the development of friction factor correlations to model two phase systems. The major contributors were those of Hagendorn and Brown (1965), Orkiszewski (1967), Aziz, Govier, and Fogarrasi (1972) and Beggs and Brill (1973). Despite the work of Hagedorn and Brown, and Orkizewski being frequently used to model oil, and gas wells, they have been seldom used for gas kick simulators since they are limited to vertical cases only. Santos (1991) is an example of a case

where Orkizewski was applied for a horizontal wellbore, however his results only focused on the difference in well control methods between vertical and horizontal wellbores and there was no code validation using experimental data. For this reason, the Beggs and Brill method has been the correlation of choice by various gas kick simulators (Avelar, 2008) because of its applicability for horizontal and inclined pipes with good results. Despite not being as accurate for vertical cases, their range for various inclinations makes them more desirable. Similar to slippage correlations, the correlations are based on limited experiments and at specific conditions, giving the potential for high error and thus the correlations may not be valid for all scenarios.

Chapter 3

Background Theory and Problem Modelling

This chapter discusses the correlations used in UTWELL and the related background theory. Furthermore, the different stages of a gas kick are discussed and how they will be modelled in UTWELL.

Since no analytical solutions exist for parameters such as density, viscosity, slip velocity between phases, frictional pressure loss factor, etc. the use of empirical correlations is required in order to obtain solutions in the simulator. This brings up the issue of discrepancy between simulators as different programs may use different correlations and consequently produce different, yet similar, results.

3.1 Governing Equations

The governing transport equations modelled by UTWELL are presented along with an explanation on their derivation and purpose.

3.1.1 Mass Conservation

The mass conservation equations are solved in order to determine the fractions of water, oil and gas that are present at any point along the wellbore. The mass conservation for the

water, oil and gas phases respectively are given by

$$\frac{\partial}{\partial t}\alpha_w\rho_w + \frac{1}{A}\frac{\partial}{\partial t}(A\alpha_w\rho_w u_w) = \dot{\psi_w} \tag{3.1}$$

$$\frac{\partial}{\partial t}\alpha_o\rho_o + \frac{1}{A}\frac{\partial}{\partial t}(A\alpha_o\rho_o u_o) = \dot{\psi_o} - \Gamma_g \tag{3.2}$$

$$\frac{\partial}{\partial t}\alpha_g\rho_g + \frac{1}{A}\frac{\partial}{\partial t}(A\alpha_g\rho_g u_g) = \dot{\psi_g} + \Gamma_g \tag{3.3}$$

where α_i, ρ_i and u_i are the holdup, density and velocity for a given phase i. $\dot{\psi_i}$ represents the source generation term for phase i. A is the area term for the analyzed gridblock and is included in order to take into account area discontinuities. Furthermore, Γ_g is the hydrocarbon interphase mass transfer between oil and gas modelled as

$$\Gamma_g = -\frac{\rho_{gsc}}{5.615B_o}\left[(\frac{\partial R_s}{\partial P})\frac{\partial P}{\partial t}\alpha_o + (\frac{\partial R_s}{\partial P})\frac{\partial P}{\partial x}\alpha_o u_o + (\frac{\partial R_s}{\partial T})\frac{\partial T}{\partial t}\alpha_o + (\frac{\partial R_s}{\partial T})\frac{\partial T}{\partial x}\alpha_o u_o\right] \tag{3.4}$$

where ρ_{gsc} is the density of gas at standard conditions, R_s is the solution gas oil ratio, B_o the formation volume factor, P is the pressure, and T is the temperature.

3.1.2 Momentum Conservation

The one dimensional Navier Stokes equation for momentum is given by

$$\begin{aligned}\frac{\partial}{\partial t}(\alpha_w\rho_w u_w + \alpha_o\rho_o u_o + \alpha_g\rho_g u_g) + \frac{\partial}{\partial x}(\alpha_w\rho_w u_w^2 + \alpha_o\rho_o u_o^2 + \alpha_g\rho_g u_g^2) + \frac{\partial P}{\partial x} \\ = -(\rho_m g_x \sin\theta + \mu\frac{\partial^2}{\partial x^2}u_x)\end{aligned} \tag{3.5}$$

where u_m is the mixture velocity of the fluid, P is the pressure along the x direction, μ is the fluid viscosity and g_x is the acceleration due to gravity along the direction of the wellbore. Θ is the angle of the wellbore with respect to the horizontal.

3.1.3 Energy

The energy equation is used to obtain the temperature distribution along the wellbore, as well as calculating the energy transfer between the wellbore and the surrounding formation. It is important to note that one of the major assumptions in UTWELL is that the individual

phases are assumed to all have the same temperature inside the wellbore, although in reality this is not the case. The energy equation used to determine the temperature of the flowing liquid in the wellbore is given by Eq 3.6.

$$\begin{aligned}
&\frac{\partial}{\partial t}\left(\alpha_w\rho_w\Big(\bar{h}_w+\frac{u_w^2}{2g_cJ_c}\Big)+\alpha_o\rho_o\Big(\bar{h}_o+\frac{u_o^2}{2g_cJ_c}\Big)+\alpha_g\rho_g\Big(\bar{h}_g+\frac{u_g^2}{2g_cJ_c}\Big)\right)+\\
&\frac{1}{A}\frac{\partial}{\partial t}\left(A\alpha_w\rho_w u_w\Big(\bar{h}_w+\frac{u_w^2}{2g_cJ_c}\Big)+A\alpha_o\rho_o u_o\Big(\bar{h}_o+\frac{u_o^2}{2g_cJ_c}\Big)+A\alpha_g\rho_g u_g\Big(\bar{h}_g+\frac{u_g^2}{2g_cJ_c}\Big)\right) \qquad (3.6)\\
&-\dot{H}_w-\dot{H}_o-\dot{H}_g+g\sin\theta\Big(\alpha_w\rho_w\frac{u_w}{g_cJ_c}+\alpha_o\rho_o\frac{u_o}{g_cJ_c}+\alpha_g\rho_g\frac{u_g}{g_cJ_c}\Big)+\frac{\dot{Q}_{loss}}{A}=0
\end{aligned}$$

where $\bar{h}_i$ is the enthalpy per unit mass of a given phase i whereas $\dot{H}_i$ are the enthalpy influxes per unit volume of phase i, g_cJ_c are unit conversion factors. The heat exchange per unit length, $\dot{Q}_{loss}$, between the fluid and formation is defined in Eq 3.7.

$$\dot{Q}_{loss}=2\pi r_{co}U_{to}(T_f-T_{wb}) \qquad (3.7)$$

U_{to} is the overall heat transfer coefficient, r_{co} is the casing outer diameter, T_f is the fluid temperature and T_{wb} is the temperature at the vicinity of the wellbore.

3.2 Single-Phase Liquid Flow

This applies to cases in the wellbore where the only flowing phase is the liquid phase, $\alpha_l = 1.0$. This occurs during normal drilling operations as well as circulation as the gas kick is flushed out of the well. Here we explore the various rheology models that could be used to model the drilling muds to be used during the simulations and their critical parameters.

3.2.1 Rheology Models

Both oil based and water based drilling muds are known to exhibit non Newtonian fluid behavior. For this reason, various rheology models are introduced into UTWELL in order to provide flexibility how the drilling fluid is modelled. This is important as the shear stress (τ) − shear strain ($\dot{\gamma}$) relationship is required to determine the frictional pressure drop

caused by the moving fluid. These are as follows:

Newtonian Fluid

The simplest of rheological models where the shear rate exerted by a fluid is directly proportional to the shear rate, as seen in Figure 3.1 The viscosity of the fluid is the gradient of the curve and remains constant. Examples of such fluids include water and honey.

$$\tau = \mu\dot{\gamma} \tag{3.8}$$

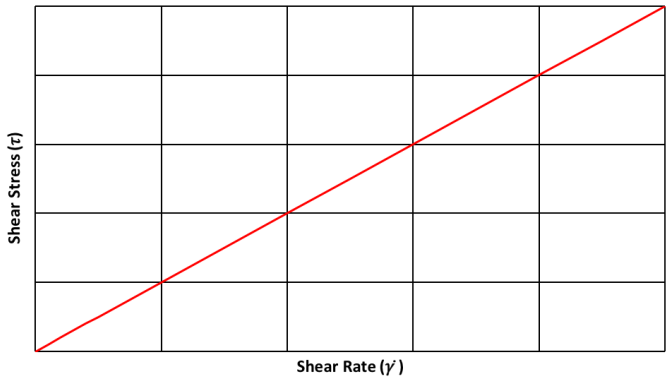

Figure 3.1: *Newtonian Fluid Shear Stress vs. Shear Strain Behaviour*

Bingham Plastic

Fluid in which a minimum shear stress (τ_y) must be met prior to inducing a shear rate, or movement. Hence, the fluid initially behaves like a solid at low shear stresses. After reaching this threshold, the relationship between shear stress and shear rate is once again constant, as seen in Figure 3.2. Common examples include drilling mud slurries and toothpaste. The behaviour is described by Eq 3.9, where τ_y is the yield point and μ_p is the plastic viscosity.

$$\tau = \tau_y + \mu_p\dot{\gamma} \tag{3.9}$$

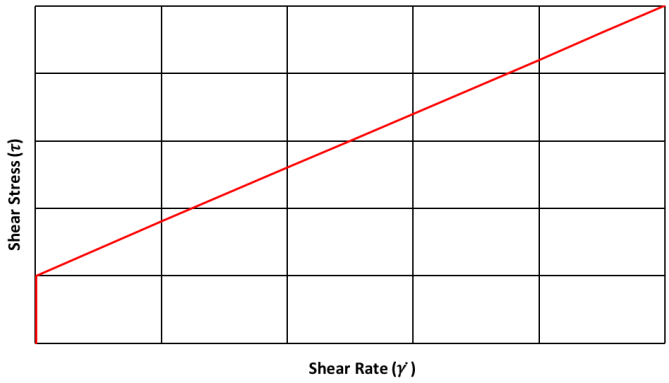

Figure 3.2: *Bingham Plastic Fluid Shear Stress vs. Shear Strain Behaviour*

Power Law

Fluid in which the shear stress behaves in a logarithmic manner as shown in Figure 3.3. It is expressed as

$$\tau = K\dot{\gamma}^N \tag{3.10}$$

where K is the flow consistency index an n is the flow behavior index. If $N > 1$, the fluid is said to be a dilatant (shear thickening) and the viscosity increases as the shear rate increases. Usually happens in fluids with suspensions. If $N < 1$, the fluid is said to be a pseudoplastic (shear-thinning) and the viscosity decreases as the shear rate increases and is usually seen in polymer solutions such as gels, as well as complex fluids such as ketchup, blood, etc.

An effective viscosity can be calculated as

$$\mu_{app} = K\dot{\gamma}^{N-1} \tag{3.11}$$

It can be seen that the special case of $N = 1$ represents a Newtonian fluid, with the apparent viscosity remaining constant.

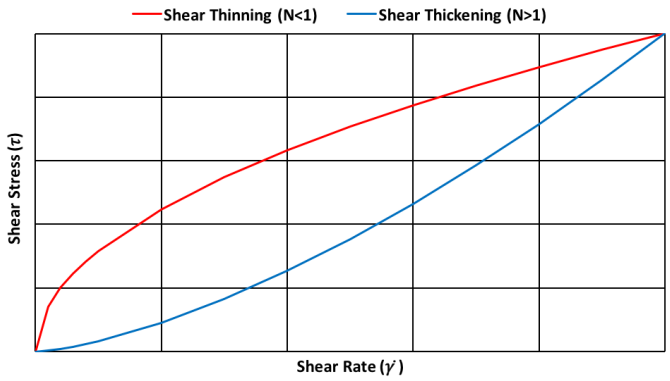

Figure 3.3: *Power Law Fluid Shear Stress vs. Shear Strain Behaviour*

3.2.2 Single-Phase Friction Factor

As seen in the momentum equation, Eq 3.5, there are two main contributors to the pressure drop experienced by fluid in a pipe: the gravitational pressure drop and frictional pressure drop. The frictional pressure drop is due to the effect of the fluids viscosity at the surface of the pipe. As the fluid moves, shear forces are exerted on the surface, generating friction, and thus requiring a higher driving force in order for the fluid to move at a given velocity. Hence, the frictional drop is a function of the kinematic viscosity of the fluid, as well as the roughness of the pipe.

Unlike 'Laminar' flow cases, no analytical solutions exist to calculate the pressure drop due to friction for 'Turbulent' flows. Thus, correlations must be used to determine the frictional loss term f. For all rheological models, the Reynolds number N_{Re}, a dimensionless parameter describing the ratio between inertial and viscous forces, is first determined. Based on the Reynolds Number, the flow is then categorized into either 'Laminar' or 'Turbulent' flow. The critical number at which transition from laminar to turbulent flow occurs is dependent on the rheological model.

Newtonian Fluid

The correlations for Newtonian fluids shown in Table 3.1 according to White (2010), with formulas adhering to SI units

	Pipe $D_h = D$	Annulus $D_h = D_o - D_i$
Reynolds Number	$N_{Re} = \frac{uD_h\rho}{\mu}$	
Laminar Flow ($N_{Re} \leq 2100$)	$f_M = \frac{64}{N_{Re}}$	
Turbulent Flow ($N_{Re} < 4000$)	$f_M \approx \left[-10 \log \left(\frac{6.9}{N_{Re}} + \left(\frac{\epsilon}{3.7 D_h} \right)^{1.11} \right) \right]^{-2}$	

Table 3.1: *Friction Factor Correlations for Newtonian Fluids*

For transitional flows, $2100 \leq N_{Re} < 4000$, linear interpolation is used. Once the moody friction factor, f_M, is calculated, the pressure drop per unit length can be calculated using Eq 3.12:

$$\frac{dP}{dL} = f_M \frac{\rho u^2}{2D_h} \tag{3.12}$$

where D_h is the equivalent hydraulic diameter. As per White (2010), this is defined as:

$$D_h = 4 \frac{Area}{Perimeter} \tag{3.13}$$

It can be shown that for a pipe D_h is equal to its diameter, whereas for an annulus it is the difference between the inner and outer diameters.

Bingham Plastic

The correlations for Bingham Plastic fluids are shown in Table 3.2 as per Bourgoyne Jr et al. (1985) and adapted for SI units.

	Pipe $D_h = D$	Annulus $D_h = D_o - D_i$
Reynolds Number	$N_{Re} = \frac{uD_h\rho}{\mu_p}$	$N_{Re} = 0.812\frac{u\rho D_h}{\mu_p}$
Laminar Flow ($N_{Re} \leq N_{Re,Crit}$)	$\frac{dP}{dL} = 32\frac{\mu_p u}{D_h^2} + \frac{16\tau_y}{3D_h}$	$\frac{dP}{dL} = 48\frac{\mu_p u}{D_h^2} + 6\frac{\tau_y}{D_h}$
Turbulent Flow ($N_{Re,Crit} < N_{Re}$)	$\frac{dP}{dL} = f_F\frac{2u^2\rho}{D_h}$	$\frac{dP}{dL} = f_F\frac{2u^2\rho}{0.816D_h}$

Table 3.2: *Friction Factor Correlations for Bingham Plastic Fluids*

where f_F is the fanning friction factor and is obtained by solving Eq. 3.14.

$$\frac{1}{f_F} = \left(4\log\left[N_{Re}f_F^{1/2}\right] - 0.4\right)^2 \tag{3.14}$$

which is the truncated Colebrook function valid for turbulent flow in smooth pipes. Note that the Fanning friction factor calculated in Eq. 3.14 and the Moody friction factor calculated in Table 3.1 are related by:

$$f_M = 4f_F \tag{3.15}$$

The Critical Reynolds number is determined by first calculating the Hedstrom number, N_{He}, using Eqs 3.16 and 3.17 for pipe and annulus geometries respectively in SI units:

$$N_{He,Pipe} = \frac{\rho\tau_y D_h^2}{\mu_p^2} \tag{3.16}$$

$$N_{He,Ann} = \frac{2}{3}\frac{\rho\tau_y D_h^2}{\mu_p^2} \tag{3.17}$$

The Critical Reynolds number, $N_{Re,Crit}$ is then determined using Eq 3.18 which has been interpolated from Bourgoyne Jr et al. (1985) and is valid for $10^3 \leq N_{He} \leq 10^7$.

$$N_{Re,Crit} = 117.4(N_{He})^{0.354} \tag{3.18}$$

Power Law

The correlations for Power Law fluids are shown in Table 3.3 adapted from Bourgoyne Jr et al. (1985), with formulas adhering to SI units. The critical Reynolds number is dependent on the power law coefficient and can be determined using Eq 3.20 and Eq 3.21.

	Pipe $D_h = D$	Annulus $D_h = D_o - D_i$
Reynolds Number	$N_{Re} = 8\frac{u^2\rho}{K}\left(\frac{D_h}{u(6+\frac{2}{N})}\right)^N$	$N_{Re} = 9.8\frac{u^2\rho}{K}\left(\frac{D_h}{u(8+\frac{4}{N})}\right)^N$
Laminar Flow ($N_{Re} \leq N_{Re,Crit}$)	$\frac{dP}{dL} = \frac{4Ku^N}{D_h^{N+1}}\left(6+\frac{2}{N}\right)^N$	$\frac{dP}{dL} = Ku^N\left(\frac{4}{D_h}\right)^{N+1}\left(2+\frac{1}{N}\right)^N$
Turbulent Flow ($N_{Re,Crit} \leq N_{Re}$)	$\frac{dP}{dL} = f_F\frac{2u^2\rho}{D_h}$	$\frac{dP}{dL} = f_F\frac{2u^2\rho}{D_h}$

Table 3.3: *Friction Factor Correlations for Power Law Fluids*

where f_F is obtained by solving Eq 3.19.

$$\frac{1}{f_F} = \left(\frac{4}{N^{0.75}}\log\left[N_{Re}f_F^{1-N/2}\right] - \frac{0.4}{N^{1.2}}\right)^2 \tag{3.19}$$

For $N_{Re,Crit}$, Eq 3.20, interpolated form Bourgoyne Jr et al. (1985), is used if $0.2 \leq N \leq 0.5$.

$$N_{Re,Crit} = 2.667 * 10^4 N^2 - 2.6 * 10^4 N + 8333 \tag{3.20}$$

If $0.5 \leq N \leq 1.0$:

$$N_{Re,Crit} = 2000 \tag{3.21}$$

3.3 Multiphase Flow

The differential equations presented in Section 3.1 only describe the governing conservation laws, however, do not take into account any slippage that may occur between the individual phases during multiphase flow. Thus, constitutive models are applied in order to determine the relative velocities of each phase to each other. For this purpose, we use the Drift Flux approach suggested by Shi et al. (2005).

3.3.1 Flow Regimes

The Drift Flux parameters, and the implemented friction factors, are heavily dependent on the flow regime that a given section of the wellbore is experiencing. For vertical anddeviated wells, four different flow regimes are considered based on the findings of Kaya, Sarica, and Brill (1999) and Taitel and Dukler (1980). The flow regime map is illustrated in Figure 3.4.

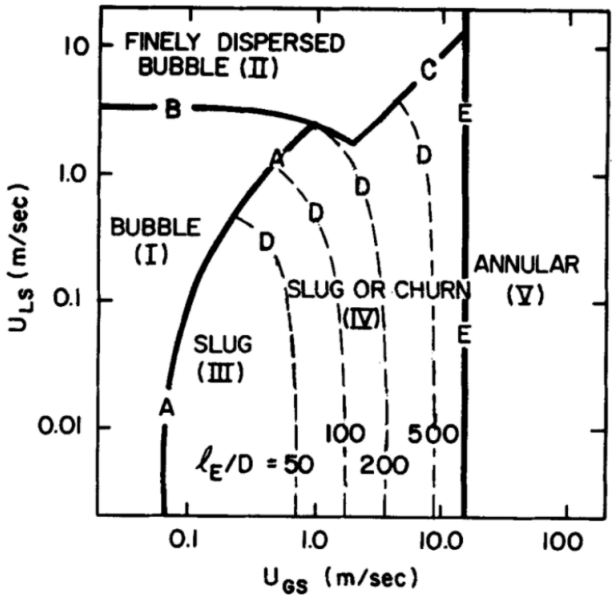

Figure 3.4: *Vertical Flow Regime as per Taitel and Dukler (1980)*

Bubbly Flow Occurs at very low gas and liquid velocities with low gas holdup content. Liquid phase dominates the gas phase, with the gas phase being discrete bubbles dispersed throughout the liquid phase. If the gas is assumed to be uniformly distributed across the liquid phase, and bubbles do not coalesce to form bigger bubbles, then slip velocity between the phased can be assumed to be low and of constant values. An increase in the velocity of the liquid phase breaks down the bubbles and changes the bubbly flow to dispersed bubbly flow.

Dispersed Bubbly Flow Dispersed bubbly flow exists in high flow rates, where strong forces break down the large bubbles into smaller ones. If the gas holdup content increases, the turbulent forces cannot prevent the unison of gas bubbles. The flow transitions into slug flow.

Slug Flow - This is the region that the flow will experience for the most part in the well. In slug flow, the gas bubbles begin to coalesce together to form large gas bubbles with in-situ velocities that are faster than that of the liquid phase, hence there is a large slip between the two phases. Since gas is moving upwards faster than the liquid phase (due to lower viscosity), then the coalesced gas bubbles can lead to a large gas holdup in a given segment, affecting the mixture density. This heavily affects the frictional pressure loss value.

Annular Flow In annular flow, the gas phase becomes the dominant phase with liquid bubbles suspended within the medium. Since the inner radius of the tubing is covered by a thin liquid film, this affects the roughness factor of the pipe since friction is occurring between the water film and the bulk fluid as opposed with the inner tube surface.

3.3.2 Drift Flux Model

In the Drift Flux Model, slippage of phases is included in the velocity correlation calculations as proposed by Hibiki and Ishii (2003). The flow regimes discussed in Section 3.3.1 determined the values of the coefficients used to determine the slip velocity.

$$u_i = C_{o,i} u_m + V_d \tag{3.22}$$

where u_i is the velocity of phase i, C_0 is a the profile parameter (distribution coefficient) of the phase, u_m is the bulk volumetric average velocity and V_d is the drift velocity. In UTWELL, u_m is determined using the momentum equation, with Eq 3.5 written as

$$\frac{\partial}{\partial t}\rho_m u_m + \frac{\partial}{\partial x}\rho_m u_m^2 + \frac{\partial P}{\partial x} = -(\rho_m g_x + \mu \frac{\partial^2}{\partial x^2} u_m) \tag{3.23}$$

The individual phase velocities, as a function of mixture velocity, are defined as follows:

$$u_g = C_{0,1}^{gl} u_m + V_{d1}^{gl} \tag{3.24}$$

$$u_l = C_{0,2}^{gl} u_m + V_{d2}^{gl} \tag{3.25}$$

$$u_o = C_{0,1}^{ow} u_m + V_{d1}^{ow} \tag{3.26}$$

$$u_w = C_{0,2}^{ow} u_m + V_{d2}^{ow} \tag{3.27}$$

Two different sets of two-phase systems are solved. The first being the two phase liquid and gas system, and the second being the oil and water slip system of the liquid phases. To determine these parameters, the correlations used by Shi et al. (2005) are used since they are suitable for the range of pipe diameters used for drilling applications. More details concerning the correlations can be found in Appendix A.

3.3.3 Two Phase Friction Factor Model

In order to determine the friction factor for the mixture velocity in two phase flow, the Beggs and Brill (1973) correlation was applied. Despite not being as accurate for vertical flows as other multiphase correlations such as Hagendorn and Brown (1965) or Orkiszewski (1967), they can be used for a wide range of well inclinations. This makes them more desirable since it provides continuity should a well have a range of inclinations. The required horizontal flow pattern map used for the correlation is the one presented by Shoham (2005) as presented in Figure 3.5.

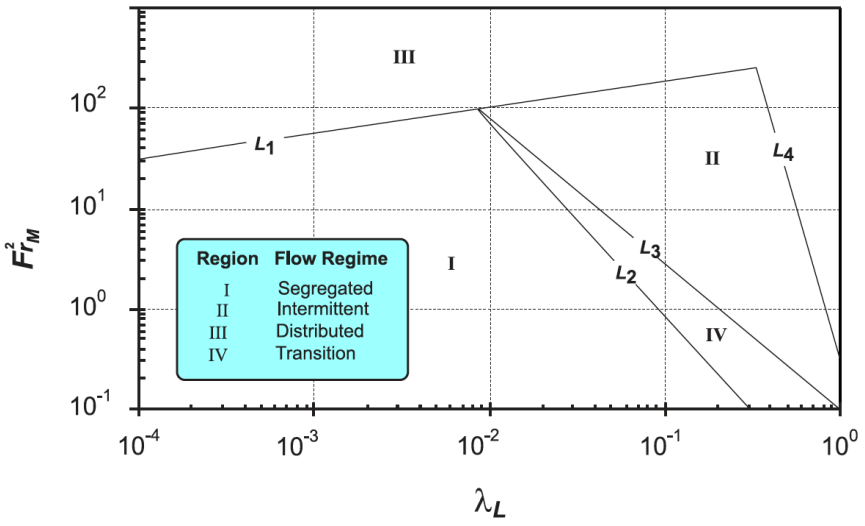

Figure 3.5: *Horizontal Flow Regime Map for Beggs and Brill Correlation Taken From Shoham (2005)*

where the dimensionless parameters, Fr_M^2 and λ_L are defined as

$$Fr_M^2 = \frac{u_m^2}{gD_h} \tag{3.28}$$

$$\lambda_L = \frac{\alpha_l u_l}{\alpha_l u_l + \alpha_g u_g} \tag{3.29}$$

Further details about the correlation can be found in Appendix B.

3.4 PVT Parameters

Fluid parameters such as density and viscosity are essential to solve the transport system of equations. Aside from ideal gas cases, there are no analytical solutions to determine these parameters and so correlations must be employed. Here we discuss the correlations implemented into the UTWELL kick simulator.

3.4.1 Density

The density of each phase is determined by calculating the Formation Volume Factor, B_i, for a given pressure and temperature along the wellbore. The density of the phase can then be determined using Eq 3.30:

$$\rho_i^* = \gamma_i \rho_{std} B_i \tag{3.30}$$

where ρ_i^* is the pressure at given conditions, γ_i is the specific gravity of the phase and ρ_{std} is the density of the phase at standard conditions and B_i is the formation volume factor of the phase. The manner in which B_i is calculated is different for the distinct phases.

Water

For the water phase, B_w is determined using the correlation suggested by McCain (1989).

Gas

The Formation Volume Factor of gas, B_g, is calculated using the Ideal Gas Law, Eq. 3.31.

$$B_i = \frac{V_{Res}}{V_{std}} = \frac{ZnRT}{P}\frac{P_{std}}{Z_{sc}nRT_{sc}} = \frac{P_{sc}ZT}{PT_{sc}} \tag{3.31}$$

where P_{sc} and T_{sc} are pressure and temperature at standard conditions. Three different correlations are implemented into UTWELL to determine the compressibility factor Z. These include the Hall and Yarborough (1973) and Dranchuk and Abou-Kassem (1975) models.

Oil

The Oil Formation Factor in UTWELL is calculated using the correlations provided by Vasquez and Beggs (1980). Since gas can dissolve into oil, this must be taken into account when determining the standard density of the oil phase, $\rho_{o,std}$:

$$\rho^*_{o,std} = \gamma_o\rho_{o,std} + \gamma_g\rho_{g,std}R_s \tag{3.32}$$

where R_s is the solution gas-oil ratio and is also determined using the Vasquez and Beggs (1980) correlation.

3.4.2 Viscosity

Water

The viscosity of the water phase is dependent on the fluid type of the drilling mud. The various viscosities of the different plasticity are illustrated in Table 3.4 for SI units.

Model	Pipe $D_h = D$	Annulus $D_h = D_o - D_i$
Newtonian	constant μ	constant μ
Bingham Plastic	$\mu_a = \mu_p + \frac{\tau_y D_h}{6u_m}$	$\mu_a = \mu_p + \frac{\tau_y D_h}{8u_m}$
Power Law	$\mu_a = \frac{KD_h}{8u_m}\left(\frac{(6+2/N)u_m}{D_h}\right)^N$	$\mu_a = \frac{KD_h}{12u_m}\left(\frac{(8+4/N)u_m}{D_h}\right)^N$

Table 3.4: *Viscosity Correlations as per Bourgoyne Jr et al. (1985)*

Gas

The correlations suggested by Standing (1977) and Lee, Gonzalez, and Eakin (1966) correlations are both implemented.

Oil

The viscosity of the oil phase is dependent on the API gravity and bubble point pressure of the prescribed oil. The various type of oil viscosities include the Undersaturated Oil Viscosity (above bubble point pressure), Live Oil Viscosity (below the bubble point pressure) and Dead oil Viscosity (at stock tank pressure). The viscocities are calculated using the Beggs and Robinson (1975), Vasquez and Beggs (1980) and De Ghetto, Paone, and Villa (1995) correlations.

3.5 Gas Kick Modelling

In this section we highlight the different stages that are to be modelled by UTWELL in order to simulate the occurrence of a gas kick. A qualitative description of the physical phenomena will be given along with the corresponding boundary conditions that are to be used by the simulator. Figure 3.6 illustrates the modelled kick stages.

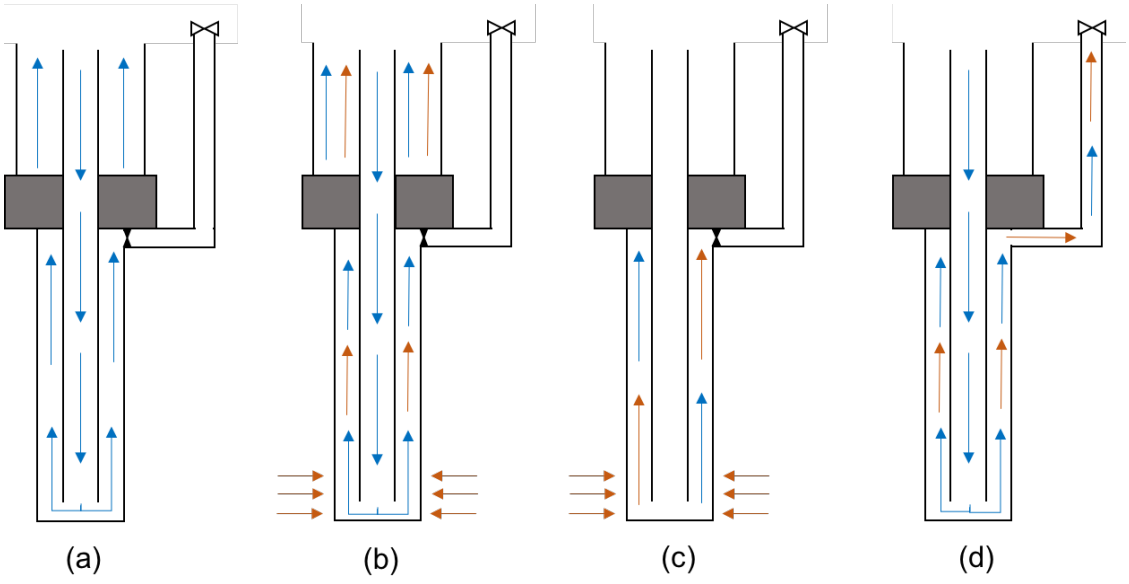

Figure 3.6: *Graphical Representation of a) Normal Drilling Operations, b) Onset of Gas kick, c) Well Shut Off and d) Recirculation Stages*

3.5.1 Gas Kick Stages

Stage 1: Normal Drilling Operations

Physical Description: Normal drilling operations are simulated. The high pressure zone has not yet been reached and hence the wellbore is operating at steady state, single-phase flow conditions.

Bottomhole Boundary Condition: *Flow.* The user inputs the flow rate at which drilling mud is being pumped at.

Surface Boundary Condition: *Pressure.* The user inputs the external pressure at the surface at which drilling mud is exiting the wellbore. In drilling operations, this would correspond to atmospheric conditions or a given wellhead pressure.

Stage 2: Onset of Gas Kick

Physical Description: The high pressure zone is reached and gas begins to enter the wellbore. The outflow rate at the surface begins to increase due to the influx of gas. The kick has not yet been identified. As gas enters the wellbore, the regime changes from single-phase to multiphase flow.

Bottomhole Boundary Condition: *Flow.* The boundary condition does not change from the boundary condition set stage 1. The drilling mud pump rate remains the same. However, the inlet of gas is positioned at one of the initial nodes (j=1,2..) and the amount of gas is determined by either Eq 3.33 or Eq 3.34 :

$$q_g = C(P_{Res} - P_{wf}) \tag{3.33}$$

where C is the user input Production Index (PI). Alternately, the PI can be defined using the reservoir parameters:

$$q_g = \frac{2\pi k_{res} h_{res}}{\mu_{g,res} ln(\frac{D_{res}}{D})}(P_{Res} - P_{wf}) \tag{3.34}$$

where k_{res}, h_{res} are the permeability and thickness of the reservoir. Additionally, a relax-

ation factor can be included in either Eq 3.33 or Eq 3.34 in order to mitigate the effects of oscillations caused by sudden introduction of the gas kick.

Surface Boundary Condition: *Pressure.* The boundary condition does not change from the boundary condition set stage 1. The kick has not yet been identified at this stage in time and hence fluid is still exiting to the User specified wellhead pressure.

Stage 3: Well Shut Off

Physical Description: The kick is identified due to the recorded pit gain. The pumps are shut off and the BOP is shut in order to contain the gas kick inside the wellbore.As the gas bubble moves along the wellbore towards the surface, the flow regime goes from single-phase to multiphase flow.

Bottomhole Boundary Condition: *Closed.* The inlet boundary condition relating to mud inflow is set to zero to simulate the shut off of the pumps. The pressure at the bottom hole is allowed to rise until the pressure is above that of the kick pressure, hence stopping the flow of gas from the reservoir.

Surface Boundary Condition: *Closed.* All velocities are set to zero in order to simulate a No Flow boundary condition. Thus this allows for the spontaneous movement of the gas bubble.

Stage 4: Re-Circulation

Physical Description: The kick is circulated out of the well by injection of drilling mud and handling of the choke valve, or any MPD method, in order to maintain a sufficient backpressure to maintain a bottomhole pressure that is higher than the kick pressure. In this Thesis, the Driller's method is applied as the gas kick is flushed out using the original mud weight.

As the recirculation front progresses through the wellbore and displaces the gas kick, the flow regime changes from multiphase back to single-phase flow.

Bottomhole Boundary Condition: *Flow.* Set to the mud recirculation rate.

Surface Boundary Condition: *Pressure.* A given wellhead pressure is set by the User. In order to induce a backpressure caused by the opening and closing of the choke valve, the following is implemented for the wellbore diameter at the last node of the grid, N:

$$D_{choke} = \beta_{open} D_N \tag{3.35}$$

Where D_N is the full diameter of the choke valve and β_{open} is the percentage of it that is open.

3.5.2 Pit Gain Modelling

The pit gain is one of the primary control methods used to make sure that drilling operations are going as expected. The main concept behind the pit gain is that under normal steady state conditions, the amount of drilling mud that enters the pit tank is equal to the amount of drilling mud being pumped back into the wellbore, hence no net volume gain. However, when a kick occurs, mass is added to this control volume. Hence, the flow rate out of the wellbore is higher than the flow rate going in. Thus, there is a net volume gain over time indicating the presence of a kick. This can be mathematically described as

$$\Delta V_{pit} = \int_0^{t_{end}} \dot{q}_{l,out} - \dot{q}_{l,in} dt \tag{3.36}$$

Eq 3.36 is discretized into Eq 3.37 in order to be implemented into UTWELL. The outlet velocity, $u_{l,out}$, is measured at the surface of the wellbore whereas the inlet velocity, $u_{l,in}$, is measured at the bottom of the wellbore. The density ratio, $\frac{\rho_{l,surf}}{\rho_{l,BHP}}$ is included in order to account for compressibility. Δt_i is the size of the time step.

$$\Delta V_{pit} = \sum_{i=1}^{t_{end}} \Big[A_{out} u_{l,out} - A_{in} u_{l,in} \big(\frac{\rho_{l,surf}}{\rho_{l,BHP}} \big) \Big] \Delta t_i \tag{3.37}$$

Chapter 4

Introduction to UTWELL

UTWELL is the wellbore production simulator, developed by Mahdy Shirdel, at The University of Texas at Austin. Using a one dimensional finite difference approach, UTWELL is capable of solving for velocity, density, pressure, temperature and phase holdup for both transient and steady state flows consisting up to three phases (water, oil and gas). Furthermore, it can be coupled with UT's compositional reservoir simulator, UTCOMP, in order to have a coupled reservoir/wellbore production simulator.

In this chapter we offer an introduction to the basic components of UTWELL, such as the finite different schemes used to discretize the main governing equations that model the physical phenomena. More information regarding UTWELL, and its' features, can be found in Shirdel (2013).

4.1 Summary of Semi Implicit Homogenous Model

The Semi Implicit Homogenous Model (SIMHM) found in UTWELL differs from conventional homogenous methods in that it has been upgraded to account for slippage effects that occur in multiphase flow phenomena. Conventional homogenous methods do not take into account slippage effects, rendering the homogenous methods unsuitable for flows with high density and viscosity contrast between the phases. This is the case in gas-liquid systems where the gas holdup is significant. Two distinct methods can be used to solve this issue, a correlative and mechanistic approach.

In the correlative approach, different sets of correlations can be used to describe the velocity of the distinct phases as a function of the bulk fluid velocity. The Drift-Flux Method is an example of such approach. Conversely, in the mechanistic approach, separate momentum equations are derived for the distinct phases and the related frictional forces between the gas and liquid phases. Correlations can then be used to describe the separate velocities of the distinct liquid and gas phases. The Two Fluid Approach is an example of such. Although various momentum equations could be setup to describe various phases, the inclusion of the additional closure equations adds challenge and complexity. This makes it more prone to instability issues, despite providing higher accuracy than the Drift Flux approach. Drift Flux methods, on the other hand, offer the advantage of being differentiable and continuous, hence making them more stable. This comes at the expense of Drift Flux Methods not being capable of handling the interphase momentum transfer between phases to the same degree as the Two Fluid Approach. However, this could be improved upon by updating the definition of the Drift Flux Parameters.

Due to simplicity and fast calculation, we opt to use the Drift Flux approach in the UTWELL gas kick simulator. However, UTWELL also includes a Semi Implicit Two Fluid (SIMPTF) that uses a similar algorithm as that for SIMHM (Shirdel and Sepehrnoori, 2017).

4.2 Numerical Discretization Method

Four transport equations are required in order to solve for four distinct unknowns: The equations to be used are:

- Water Mass Conservation
- Mixture Mass Difference Conservation
- Mixture Mass Conservation
- Momentum Conservation

For discretization of the wellbore space, a staggered grid approach, as seen in Figure 4.2, is employed. Junctions between nodes are labelled with K, L and M designation whereas

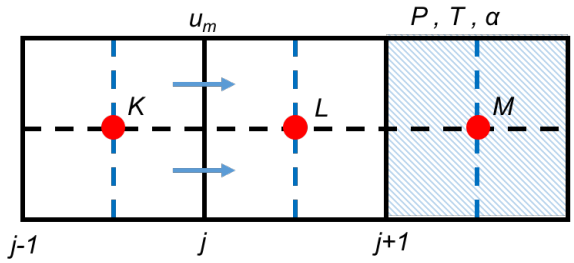

Figure 4.1: *Schematic of Discretized Staggered Grid Approach*

grid block centers are labelled using a j index. Velocities are calculated at the junctions whereas pressure, temperature and holdups are calculated at the gridblock centers.

The Transport equations are discretized using forward difference schemes and any nonlinearities are backdated. The implicit variables have been selected to improve stability of the system (Shirdel (2013)). The physical equations, along with their discretization, are presented:

4.2.1 Water Mass Conservation

$$\frac{\partial}{\partial t}\alpha_w\rho_w + \frac{\partial}{\partial x}\alpha_w\rho_w u_w = \dot{\psi_w} \tag{4.1}$$

$$\begin{aligned} &V_b[\rho^n(\tilde{\alpha}^{n+1}_{w,j} - \alpha^n_{w,j}) - \alpha^n_w(\tilde{\rho}^{n+1}_{w,j} - \rho^n_{w,j})]+ \\ &\Delta t[\dot{\alpha}^n_{w,j+1}\dot{\rho}^n_{w,j+1}A^n_{w,j+1}u^{n+1}_{w,j+1} - \dot{\alpha}^n_{w,j}\dot{\rho}^n_{w,j}A^n_{w,j}u^{n+1}_{w,j}] = V_b\Delta t\dot{\psi}^n_{w,j} \end{aligned} \tag{4.2}$$

4.2.2 Mixture Mass Difference Conservation

$$\frac{\partial}{\partial t}(\alpha_g\rho_g - \alpha_o\rho_o - \alpha_w\rho_w) + \frac{\partial}{\partial x}(\alpha_g\rho_g u_g - \alpha_o\rho_o u_o - \alpha_w\rho_w u_w) = 2\Gamma_g + \dot{\psi_g} - \dot{\psi_o} - \dot{\psi_w} \tag{4.3}$$

$$\begin{aligned} &V_b[\rho^n_g(\tilde{\alpha}^{n+1}_{g,j} - \alpha^n_{g,j}) - \rho^n_o(\tilde{\alpha}^{n+1}_{o,j} - \alpha^n_{o,j}) - \rho^n_w(\tilde{\alpha}^{n+1}_{w,j} - \alpha^n_{w,j})]- \\ &V_b[\alpha^n_g(\tilde{\rho}^{n+1}_{g,j} - \rho^n_{g,j}) - \alpha^n_o(\tilde{\rho}^{n+1}_{o,j} - \rho^n_{o,j}) - \alpha^n_w(\tilde{\rho}^{n+1}_{w,j} - \rho^n_{w,j})]+ \\ &\Delta t[\dot{\alpha}^n_{g,j+1}\dot{\rho}^n_{g,j+1}A^n_{g,j+1}u^{n+1}_{g,j+1} - \dot{\alpha}^n_{g,j}\dot{\rho}^n_{g,j}A^n_{g,j}u^{n+1}_{g,j}]- \\ &\Delta t[\dot{\alpha}^n_{o,j+1}\dot{\rho}^n_{o,j+1}A^n_{o,j+1}u^{n+1}_{o,j+1} - \dot{\alpha}^n_{o,j}\dot{\rho}^n_{o,j}A^n_{o,j}u^{n+1}_{o,j}]- \\ &\Delta t[\dot{\alpha}^n_{w,j+1}\dot{\rho}^n_{w,j+1}A^n_{w,j+1}u^{n+1}_{w,j+1} - \dot{\alpha}^n_{w,j}\dot{\rho}^n_{w,j}A^n_{w,j}u^{n+1}_{w,j}] \\ &= V_b\Delta t(2\Gamma_g + \dot{\psi}^n_{g,j} - \dot{\psi}^n_{o,j} - \dot{\psi}^n_{w,j}) \end{aligned} \tag{4.4}$$

4.2.3 Mixture Mass Conservation

$$\frac{\partial}{\partial t}(\alpha_g\rho_g + \alpha_o\rho_o + \alpha_w\rho_w) + \frac{\partial}{\partial x}(\alpha_g\rho_g u_g + \alpha_o\rho_o u_o + \alpha_w\rho_w u_w) = \dot{\psi_g} + \dot{\psi_o} + \dot{\psi_w} \tag{4.5}$$

$$\begin{aligned}
&V_b[\rho_g^n(\tilde{\alpha}_{g,j}^{n+1} - \alpha_{g,j}^n) + \rho_o^n(\tilde{\alpha}_{o,j}^{n+1} - \alpha_{o,j}^n) + \rho_w^n(\tilde{\alpha}_{w,j}^{n+1} - \alpha_{w,j}^n)]- \\
&V_b[\alpha_g^n(\tilde{\rho}_{g,j}^{n+1} - \rho_{g,j}^n) + \alpha_o^n(\tilde{\rho}_{o,j}^{n+1} - \rho_{o,j}^n) + \alpha_w^n(\tilde{\rho}_{w,j}^{n+1} - \rho_{w,j}^n)]+ \\
&\Delta t[\dot{\alpha}_{g,j+1}^n\dot{\rho}_{g,j+1}^n A_{g,j+1}^n u_{g,j+1}^{n+1} - \dot{\alpha}_{g,j}^n\dot{\rho}_{g,j}^n A_{g,j}^n u_{g,j}^{n+1}]+ \\
&\Delta t[\dot{\alpha}_{o,j+1}^n\dot{\rho}_{o,j+1}^n A_{o,j+1}^n u_{o,j+1}^{n+1} - \dot{\alpha}_{o,j}^n\dot{\rho}_{o,j}^n A_{o,j}^n u_{o,j}^{n+1}]+ \\
&\Delta t[\dot{\alpha}_{w,j+1}^n\dot{\rho}_{w,j+1}^n A_{w,j+1}^n u_{w,j+1}^{n+1} - \dot{\alpha}_{w,j}^n\dot{\rho}_{w,j}^n A_{w,j}^n u_{w,j}^{n+1}] \\
&= V_b\Delta t(\dot{\psi}_{g,j}^n + \dot{\psi}_{o,j}^n + \dot{\psi}_{w,j}^n)
\end{aligned} \tag{4.6}$$

4.2.4 Momentum Conservation

$$\frac{\partial}{\partial t}\rho_m u_m + \frac{\partial}{\partial x}\rho_m u_m^2 + \frac{\partial P}{\partial x} + \rho_m g\sin\theta + F_f = \dot{\psi_g} + \dot{\psi_o} + \dot{\psi_w} \tag{4.7}$$

$$\begin{aligned}
&\Delta x_j[\rho_{m,j+1}^{n+1}u_{m,j+1}^{n+1} - \rho_{m,j}^n u_{m,j}^n] + \Delta t[\rho_{m,j}^n(u_{m,L}^n)^2 - \rho_{m,j}^n(u_{m,M}^n)^2] = \\
&- \Delta t144g_c[P_j^{n+1} - P_{j-1}^{n+1}] - \frac{1}{2}\frac{f_M\rho_{m,j}^n|u_{m,j}^n|}{D_j^n}u_{m,j}^{n+1} - \Delta t\Delta x_j\rho_{m,j}^n g_c sin\theta \\
&+ \Delta t\Delta x(\dot{\psi}_{g,j}^n + \dot{\psi}_{o,j}^n + \dot{\psi}_{w,j}^n)
\end{aligned} \tag{4.8}$$

4.3 Algorithm

This section focuses on the algorithm used for the SIMHM, for a full detailed version of the derivations of each matrix, see Appendix C. First, Equations 4.2, 4.4 and 4.6 are setup as functions of water holdup, gas holdup, pressure change and mixture velocity as shown in Eq 4.9. The primary goal is solve for P, $\tilde{\alpha}_w$ and $\tilde{\alpha}_g$ which represent presure, and the provisional advanced water and gas volume fractions respectively.

$$\begin{aligned}
&A(I,1)(\tilde{\alpha}_{w,j}^{n+1} - \alpha_{w,j}^n) + A(I,2)(\tilde{\alpha}_{g,j}^{n+1} - \alpha_{g,j}^n) + A(I,3)(P_j^{n+1} - P_j^n) = \\
&B(I) + u_{m,j+1}^{n+1}M_1(I) + u_{m,j}^{n+1}M_0(I)
\end{aligned} \tag{4.9}$$

I=1: Water Mass Conservation

I=2: Mass Difference Conservation

I=3: Water Summation Conservation

The discretized momentum conservation equation, Eq 4.8, is rearranged as a function of mixture velocity and the pressure change across the node:

$$u_{m,j}^{n+1}X(I) = Y(1) + Z(1)(P_j^{n+1} - P_{j-1}^{n+1}) \tag{4.10}$$

Substitute Eq 4.10 into Eq 4.9 for $u_{m,j+1}^{n+1}$ and $u_{m,j}^{n+1}$

$$\begin{aligned} A(I,1)(\tilde{\alpha}_{w,j}^{n+1} - \alpha_{w,j}^{n}) + A(I,2)(\tilde{\alpha}_{g,j}^{n+1} - \alpha_{g,j}^{n}) + A(I,3)(P_j^{n+1} - P_j^n) = \\ B(I) + M_1(I)[X^{-1}Y(1) + X^{-1}Z(1)(P_{j+1}^{n+1} - P_j^{n+1})] + \\ M_0(I)[X^{-1}Y(1) + X^{-1}Z(1)(P_j^{n+1} - P_{j-1}^{n+1})] \end{aligned} \tag{4.11}$$

Decoupling for Pressure (*I=3*)

$$\begin{aligned} (P_j^{n+1} - P_j^n) = & A^{-1}B(3) + A^{-1}M_1(3)[X^{-1}Y(1) + X^{-1}Z(1)(P_{j+1}^{n+1} - P_j^{n+1})] + \\ & A^{-1}M_0(3)[X^{-1}Y(1) + X^{-1}Z(1)(P_j^{n+1} - P_{j-1}^{n+1})] \end{aligned} \tag{4.12}$$

The above equation is written for nodes *L=2* to *L=N-1*. At the boundary nodes *(L=1,L=N)*, certain modifications are made dependent on whether the boundaries are Pressure or Flow Nodes. For a Flow boundary at the inlet, Eq 4.12 becomes:

$$\begin{aligned} (P_1^{n+1} - P_1^n) = & A^{-1}B(3) + A^{-1}M_1(3)[X^{-1}Y(1) + X^{-1}Z(1)(P_2^{n+1} - P_1^{n+1})] + \\ & A^{-1}M_0(3)[u_{m,Inlet}] \end{aligned} \tag{4.13}$$

For Pressure boundary condition at the outlet:

$$\begin{aligned} (P_N^{n+1} - P_N^n) = & A^{-1}B(3) + A^{-1}M_1(3)[X^{-1}Y(1) + X^{-1}Z(1)(P_{Outlet} - P_N^{n+1})] + \\ & A^{-1}M_0(3)[X^{-1}Y(1) + X^{-1}Z(1)(P_N^{n+1} - P_{N-1}^{n+1})] \end{aligned} \tag{4.14}$$

The Closed boundary condition is a special case of the Flow condition where $u_{m,Inlet}$ or $u_{m,Outlet}$ are set to zero. Setting up Eq 4.12 for all nodes leads to the formation of a tri-diagonal matrix that when solved yields the pressure values for all nodes along the wellbore. Once Pressure is solved, $u_{m,j}^{n+1}$ is determined using Eq 4.10. Subsequently, the water, oil and gas velocities are determined using the Drift Flux correlations.

With the newly calculated velocity and pressure values for each node, the provisional future gas and liquid holdup values, $\alpha_{w,L}^{\tilde{n+1}}$ and $\alpha_{g,L}^{\tilde{n+1}}$, are determined using Eq.4.9 by uncoupling for the holdups, similar to what was done in Eq. 4.12 for pressure. Lastly, the actual phasic volume fractions are determined. First, the total masses of each phase per grid block are determined using the mass conservation equation of each phase:

$$\begin{aligned}(\rho_w\alpha_w)_L^{n+1} =&(\rho_w\alpha_w)_L^n + \frac{\Delta t}{V_b}[\dot{\alpha}_{w,j+1}^n\dot{\rho}_{w,j-1}^n A_{w,j-1}^n u_{w,j-1}^{n+1} - \dot{\alpha}_{w,j}^n\dot{\rho}_{w,j}^n A_{w,j}^n u_{w,j}^{n+1}] \\ &+ V_b\Delta t\dot{\psi}_{w,j}^n\end{aligned} \tag{4.15}$$

$$\begin{aligned}(\rho_o\alpha_o)_L^{n+1} =&(\rho_o\alpha_o)_L^n + \frac{\Delta t}{V_b}[\dot{\alpha}_{o,j+1}^n\dot{\rho}_{o,j-1}^n A_{o,j-1}^n u_{o,j-1}^{n+1} - \dot{\alpha}_{o,j}^n\dot{\rho}_{o,j}^n A_{o,j}^n u_{o,j}^{n+1}] \\ &+ V_b\Delta t\dot{\psi}_{o,j}^n\end{aligned} \tag{4.16}$$

$$\begin{aligned}(\rho_g\alpha_g)_L^{n+1} =&(\rho_g\alpha_g)_L^n + \frac{\Delta t}{V_b}[\dot{\alpha}_{g,j+1}^n\dot{\rho}_{g,j-1}^n A_{g,j-1}^n u_{g,j-1}^{n+1} - \dot{\alpha}_{g,j}^n\dot{\rho}_{g,j}^n A_{g,j}^n u_{g,j}^{n+1}] \\ &+ V_b\Delta t\dot{\psi}_{g,j}^n\end{aligned} \tag{4.17}$$

The actual phase holdups are then calculated:

$$(\alpha_w)_L^{n+1} = \frac{(\rho_w\alpha_w)_L^{n+1}}{\tilde{\alpha}_{w,L}^{n+1}} \tag{4.18}$$

$$(\alpha_g)_L^{n+1} = \frac{(\rho_g\alpha_g)_L^{n+1}}{\tilde{\alpha}_{g,L}^{n+1}} \tag{4.19}$$

$$(\alpha_o)_L^{n+1} = 1 - (\alpha_g)_L^{n+1} - (\alpha_w)_L^{n+1} \tag{4.20}$$

The sum of volume fraction values are checked to ensure they are equal to 1.The new PVT parameters are then calculated using the new updated variables.

If temperature is to be calculated for non-isothermal conditions, Newton-Raphson iterative approach is employed in order to calculate the temperature along the wellbore implicitly. This is done by setting the discretized energy equation as a residual, as shown in Eq 4.22, and constructing a Jacobian matrix composed of the derivative of the energy equation with respect to temperature (Eq 4.21).

$$J_T = \begin{bmatrix} \frac{\partial R_{T,1}}{\partial T_1} & \frac{\partial R_{T,1}}{\partial T_2} & 0 & ... & 0 \\ \frac{\partial R_{T,2}}{\partial T_1} & \frac{\partial R_{T,2}}{\partial T_2} & \frac{\partial R_{T,2}}{\partial T_3} & 0 & 0 \\ 0 & \frac{\partial R_{T,i}}{\partial T_{i-1}} & \frac{\partial R_{T,i}}{\partial T_i} & \frac{\partial R_{T,i}}{\partial T_{i+1}} & 0 \\ 0 & 0 & \frac{\partial R_{T,N-1}}{\partial T_{N-2}} & \frac{\partial R_{T,N-1}}{\partial T_N - 1} & \frac{\partial R_{T,N-1}}{\partial T_N} \\ 0 & 0 & 0 & \frac{\partial R_{T,N}}{\partial T_{N-1}} & \frac{\partial R_{T,N}}{\partial T_N} \end{bmatrix} \tag{4.21}$$

$$\begin{aligned} R_T = {} & V_b \left[\dot{\alpha}_{w,L}^{n+1} \dot{\rho}_{w,L}^{n+1} \left(\dot{\bar{h}}_{w,L}^{n+1} + \frac{(u_w^2)_j^{n+1}}{2 g_c J_c} \right) - \dot{\alpha}_{w,L}^{n} \dot{\rho}_{w,L}^{n} \left(\dot{\bar{h}}_{w,L}^{n} + \frac{(u_w^2)_j^{n}}{2 g_c J_c} \right) \right] + \\ & V_b \left[\dot{\alpha}_{o,L}^{n+1} \dot{\rho}_{o,L}^{n+1} \left(\dot{\bar{h}}_{o,L}^{n+1} + \frac{(u_o^2)_j^{n+1}}{2 g_c J_c} \right) - \dot{\alpha}_{o,L}^{n} \dot{\rho}_{o,L}^{n} \left(\dot{\bar{h}}_{o,L}^{n} + \frac{(u_o^2)_j^{n}}{2 g_c J_c} \right) \right] + \\ & V_b \left[\dot{\alpha}_{g,L}^{n+1} \dot{\rho}_{g,L}^{n+1} \left(\dot{\bar{h}}_{g,L}^{n+1} + \frac{(u_g^2)_j^{n+1}}{2 g_c J_c} \right) - \dot{\alpha}_{g,L}^{n} \dot{\rho}_{g,L}^{n} \left(\dot{\bar{h}}_{g,L}^{n} + \frac{(u_g^2)_j^{n}}{2 g_c J_c} \right) \right] + \\ & \Delta t \left[A_j^n \dot{\alpha}_{w,L}^{n+1} \dot{\rho}_{w,L}^{n+1} u_{j,L}^{n+1} \left(\dot{\bar{h}}_{w,L}^{n+1} + \frac{(u_w^2)_j^{n+1}}{2 g_c J_c} \right) - A_{j-1}^n \dot{\alpha}_{w,K}^{n+1} \dot{\rho}_{w,K}^{n+1} u_{w,j-1}^{n+1} \left(\dot{\bar{h}}_{w,K}^{n+1} + \frac{(u_w^2)_{j-1}^{n+1}}{2 g_c J_c} \right) \right] + \\ & \Delta t \left[A_j^n \dot{\alpha}_{o,L}^{n+1} \dot{\rho}_{o,L}^{n+1} u_{o,j}^{n+1} \left(\dot{\bar{h}}_{o,L}^{n+1} + \frac{(u_o^2)_j^{n+1}}{2 g_c J_c} \right) - A_{j-1}^n \dot{\alpha}_{o,K}^{n+1} \dot{\rho}_{o,K}^{n+1} u_{o,j-1}^{n+1} \left(\dot{\bar{h}}_{o,K}^{n+1} + \frac{(u_o^2)_{j-1}^{n+1}}{2 g_c J_c} \right) \right] + \\ & \Delta t \left[A_j^n \dot{\alpha}_{g,L}^{n+1} \dot{\rho}_{g,L}^{n+1} u_{g,j}^{n+1} \left(\dot{\bar{h}}_{g,L}^{n+1} + \frac{(u_g^2)_j^{n+1}}{2 g_c J_c} \right) - A_{j-1}^n \dot{\alpha}_{g,K}^{n+1} \dot{\rho}_{g,K}^{n+1} u_{g,j-1}^{n+1} \left(\dot{\bar{h}}_{g,K}^{n+1} + \frac{(u_g^2)_{j-1}^{n+1}}{2 g_c J_c} \right) \right] - \\ & V_b \left[\dot{H}_{w,L}^{n+1} - \dot{H}_{o,L}^{n+1} - \dot{H}_{g,L}^{n+1} \right] + V_b \Delta t \left[\frac{\dot{Q}_{loss,L}^n}{A_j^n} \right] + \\ & V_b g sin\theta \Delta t \left[\alpha_{w,L}^{n+1} \rho_{w,L}^{n+1} \frac{u_{w,L}^{n+1}}{g_c J_c} + \alpha_{o,L}^{n+1} \rho_{o,L}^{n+1} \frac{u_{o,L}^{n+1}}{g_c J_c} + \alpha_{g,L}^{n+1} \rho_{g,L}^{n+1} \frac{u_{g,L}^{n+1}}{g_c J_c} \right] \end{aligned} \tag{4.22}$$

The final temperature is calculated via Eq 4.23.

$$T^{n+1} = T^n - J_T^{-1} R_T \tag{4.23}$$

Once temperature has been determined the time step is determined for the proceeding iteration.

4.4 Time Step Control

For semi-implicit difference schemes, calculation of the time step is crucial to achieving convergence in the solution. In UTWELL, first the residual masses for each grid block are calculated using Eqs 4.24 and 4.25.

$$\rho_{ms,L}^{n+1} = (\alpha_{w,L}^{n+1}\rho_{w,L}^{n+1}) + (\alpha_{o,L}^{n+1}\rho_{o,L}^{n+1}) + (\alpha_{g,L}^{n+1}\rho_{g,L}^{n+1}) \tag{4.24}$$

$$\rho_{mt,L}^{n+1} = (\alpha_w\rho_w)_L^{n+1} + (\alpha_o\rho_o)_L^{n+1} + (\alpha_g\rho_g)_L^{n+1} \tag{4.25}$$

Then, the residual and squared residual mass errors are determined using Eqs 4.26 and 4.27.

$$\epsilon_m = \frac{max(|\rho_{ms,L}^{n+1} - \rho_{mt,L}^{n+1}|)}{\rho_{ms,L}^{n+1}} \tag{4.26}$$

$$\epsilon_{rms} = \frac{2\sum_{L=1}^{N}[V_{b,L}(\rho_{ms,L}^{n+1} - \rho_{mt,L}^{n+1})]^2}{\sum_{L=1}^{N}(\rho_{ms,L}^{n+1})^2} \tag{4.27}$$

The time step is then defined using the following criteria

URME$< \epsilon_m, \epsilon_{rms}$	$\Delta t_{new} = \frac{1}{2}\Delta t_{old}$
LRME$< \epsilon_m, \epsilon_{rms} < URME$	$\Delta t_{new} = \Delta t_{old}$
$\epsilon_m, \epsilon_{rms} < LRME$	$\Delta t_{new} = 2\Delta t_{old}$

URME and LRME are the upper and lower residual mass error parameters usually set as 8*10-3 and 8*10-4 respectively. Once the time step has been determined, the algorithm is then repeated until the required simulation time is reached. This method allows for proper convergence as it assures that the residual mass calculated in Eqs 4.15, 4.16 and 4.17 do not differ significantly from the product of the independently calculated holdup and density values as calculated through Eqs 4.18, 4.19, 4.20 and the PVT correlations.

4.5 General Algorithm

Figures 4.2 and 4.3 present a visual representation of the entire SIMPHM and gas kick algorithm for one time step as performed in UTWELL.

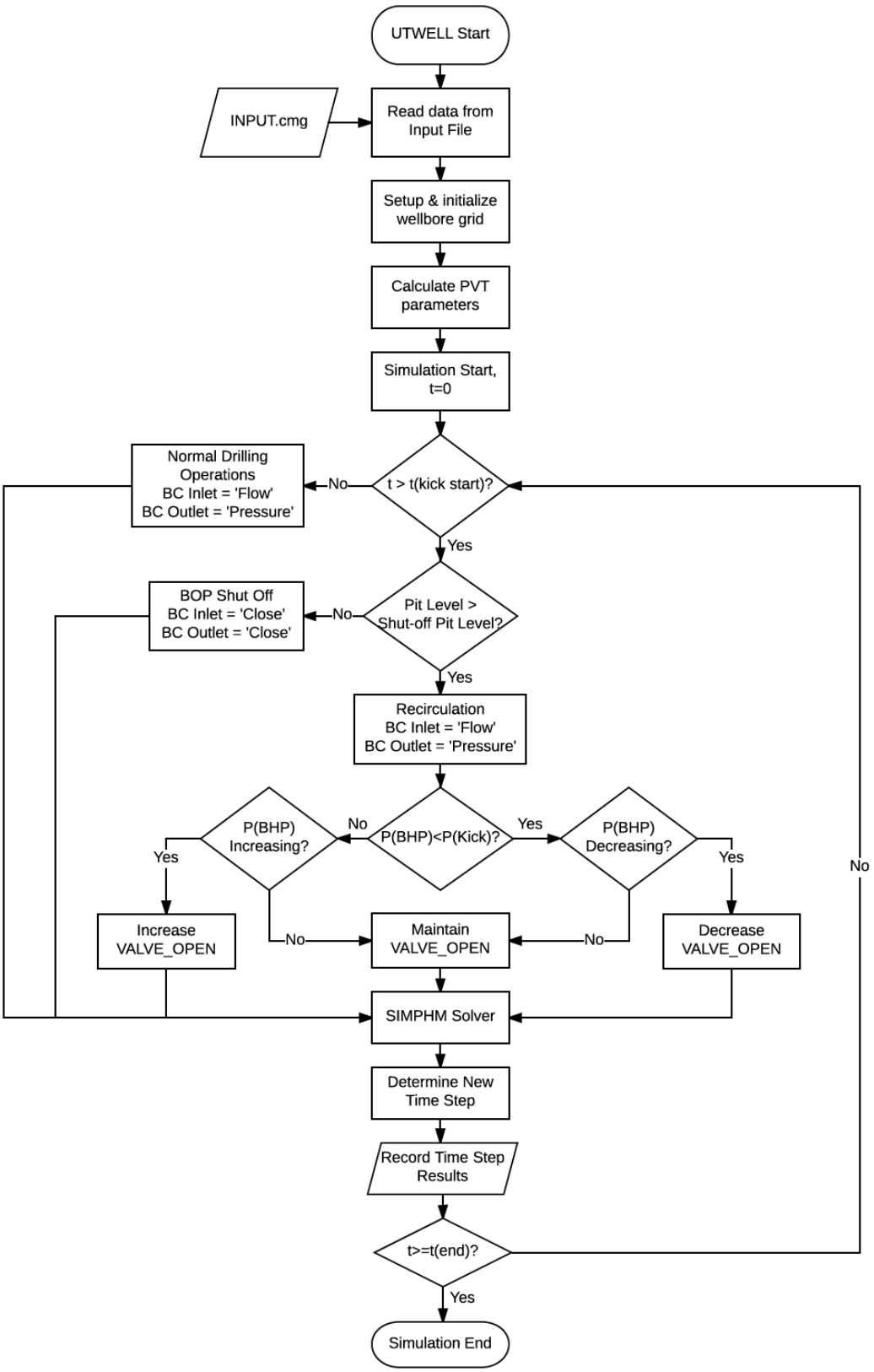

Figure 4.2: *Flowchart of UTWELL Gas Kick Algorithm*

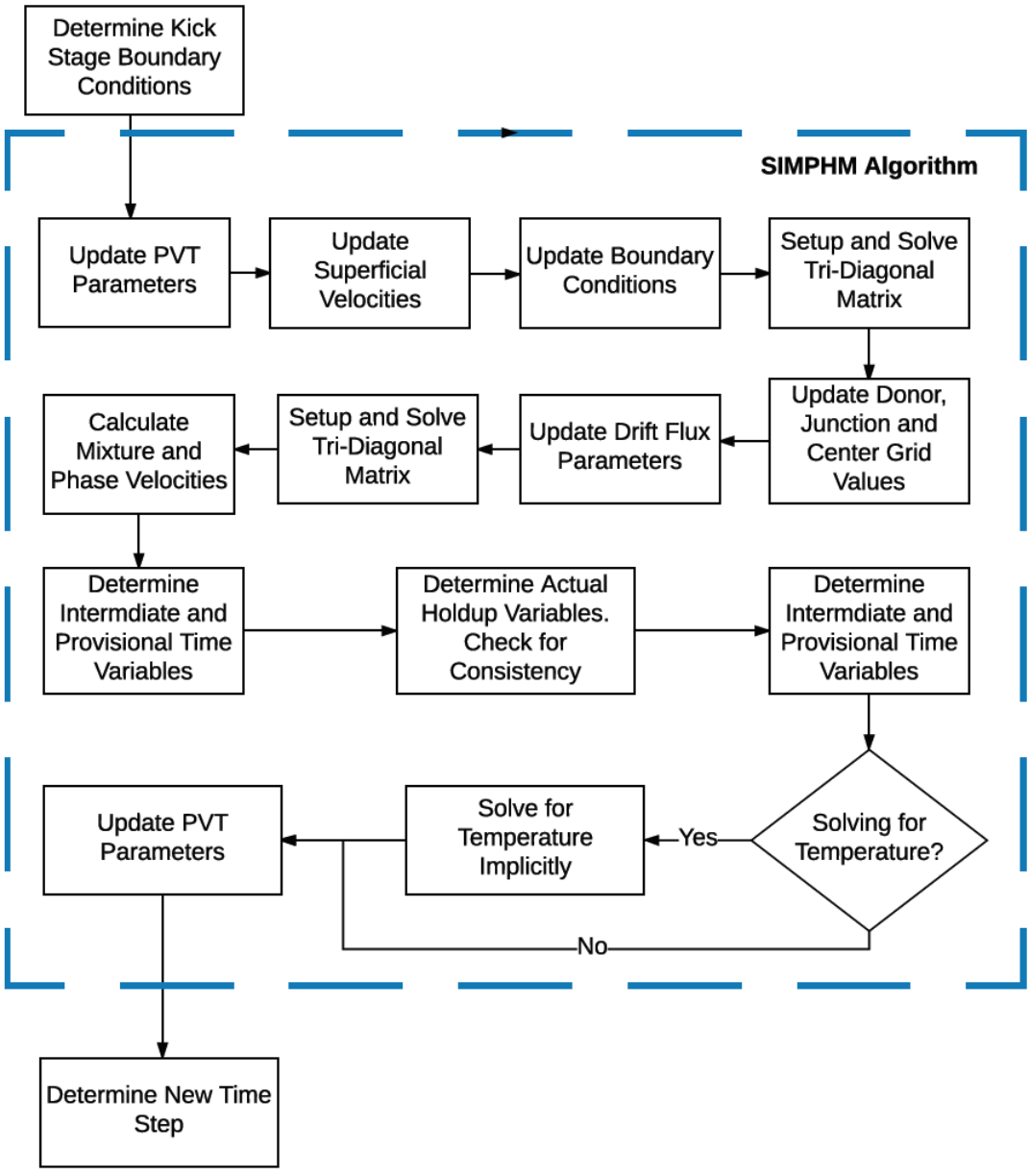

Figure 4.3: *Flowchart of SIMPHM Solver Algorithm*

Chapter 5

Case Studies and Results

Here the results produced by the UTWELL Gas Kick simulator are presented. We begin by presenting simple, analytic cases in order to demonstrate the robustness of the simulator before proceeding with more complicated, test cases.

5.1 Single-Phase Cases

The first set of tests are to determine whether or not the simulator can handle single-phase problems and produce steady state results to good accuracy. These are benchmarked with the analytic solutions to determine the accuracy of the simulator.

The simulator is tested for the flow of mud in a 1,000 ft well for both laminar and turbulent flows. Only flow in an annulus will be tested. This is because the algorithm and formulae for both pipe and annular cases are the same, however the procedure for annular flow is more sensitive due to the calculation of the area of the annulus. Thus, if the simulator works for annular situations, it will work for pipe flow. Additionally, each simulation is done twice. One simulation will assume non compressible flow (i.e ρ_w is constant for all P and T) and one assuming compressible flow. This is done in order to gain an appreciation for the effect of compressibility in calculations, and to determine whether analytical solutions could be used as suitable benchmarks for more complicated results further on.

5.1.1 Single-Phase Newtonian Flow

Density (ppg)	8.34
Viscosity (cP)	1

Table 5.1: *Fluid Data for Newtonian Single-Phase Flow Simulations*

Well Depth (ft)	1,000
Wellbore ID (in)	6
Drillstring OD (in)	3
Laminar Flow Rate (gpm)	5
Turbulent Flow Rate (gpm)	500

Table 5.2: *Well Data for Newtonian Single-Phase Annulus Flow Simulation*

ΔP (psi)	Static Pressure	Frictional Pressure
Analytical Solution	433.16	0.00561
Non Compressible Simulation	433.58	0.00562
Compressible Simulation	434.57	0.00562

Table 5.3: *Pressure Difference Results for Newtonian Single-Phase Laminar Flow Simulation*

ΔP (psi)	Static Pressure	Frictional Pressure
Analytical Solution	433.16	24.49
Non Compressible Simulation	433.58	26.26
Compressible Simulation	434.57	26.43

Table 5.4: *Pressure Difference Results for Single-Phase Newtonian Turbulent Flow Simulation*

5.1.2 Single-Phase Bingham Plastic

Density (ppg)	10.0
Yield Point (lbf.100sqft^{-1})	15
Plastic Viscosity (cP)	40

Table 5.5: *Fluid Data for Bingham Plastic Single-Phase Flow Simulations*

Well Depth (ft)	1,000
Wellbore ID (in)	6.5
Drillstring OD (in)	4.5
Laminar Flow Rate (gpm)	200
Turbulent Flow Rate (gpm)	600

Table 5.6: *Well Data for Bingham Plastic Single-Phase Simulation*

ΔP (psi)	Static Pressure	Frictional Pressure
Analytical Solution	520	74.63
Non Compressible Simulation	520.3	74.70
Compressible Simulation	521.84	74.79

Table 5.7: *Pressure Difference Results for Single-Phase Bingham Plastic Laminar Flow Simulation*

ΔP (psi)	Static Pressure	Frictional Pressure
Analytical Solution	520	289
Non Compressible Simulation	520.3	289.39
Compressible Simulation	522.4	292.22

Table 5.8: *Pressure Difference Results for Single-Phase Bingham Plastic Turbulent Flow Simulation*

5.1.3 Single-Phase Power Law

Density (ppg)	15.6
Consistency Index (eq cP)	335
Flow Behaviour Index (cP)	0.67

Table 5.9: *Fluid Data for Power Law Single-Phase Flow Simulations*

Well Depth (ft)	1,000
Wellbore ID (in)	9.625
Drillstring OD (in)	7.0
Laminar Flow Rate (gpm)	200
Turbulent Flow Rate (gpm)	672

Table 5.10: *Well Data for Bingham Plastic Single-Phase Simulation*

ΔP (psi)	Static Pressure	Frictional Pressure
Analytical Solution	811.2	21.87
Non Compressible Simulation	810.8	21.89
Compressible Simulation	814.15	21.94

Table 5.11: *Pressure Difference Results for Single-Phase Power Law Laminar Flow Simulation*

ΔP (psi)	Static Pressure	Frictional Pressure
Analytical Solution	811.2	91
Non Compressible Simulation	810.8	89.65
Compressible Simulation	814.43	90.58

Table 5.12: *Pressure Difference Results for Single-Phase Power Law Turbulent Flow Simulation*

As can be seen, the results produced by UTWELL are in agreement with the analytical solution. For all three cases, the compressible solution had slightly higher static and frictional pressures. This is expected due to the increase in density of the fluid at higher pressures. Since both static pressure and frictional pressure are proportional to density, it will lead to higher values. It was also observed that discrepancies between the analytical and simulated solution were higher for turbulent cases. This could simply be due to the fact that the solutions for turbulent flows are highly dependent on correlations, and hence more prone to deviations.

The discrepancies in general were not significant, showing UTWELL is capable of simulating single-phase flow in a wellbore for different mud rheologies. Furthermore, the differences between the compressible and non compressible simulations were minor, meaning that the use of analytical, non compressible solutions for the liquid phase could be used as a suitable benchmark for upcoming tests.

5.2 Well Discontinuities

Discontinuities in the annulus of a drilling wellbore are to be expected in real life applications. This is especially true for deep wells that require the use of various casings or risers, for offshore wells. Despite their prevalence, there are limited publications where a wellbore simulator with discontinuities has been tested for code verification. Of the few, Udegbunam et al. (2015) provide various hypothetical studies.

In this section we test the robustness of the code to handle such discontinuities for both single-phase and multiphase cases. First a hypothetical well with various discontinuities is tested for single-phase. Then we compare with one of the hypothetical tests performed by Udegbunam et al. (2015) to test for consistency and whether UTWELL can handle multiphase gas kick tests. In both cases, the PVT data and correlations used are shown in Table 5.13 and Eqs. 5.1 and 5.2 in order to be consistent with Udegbunam et al. (2015).

$$\rho_l = \rho_0 + \frac{p - p_0}{\alpha_l^2} \tag{5.1}$$

$$\rho_g = \frac{p}{\alpha_g^2} \tag{5.2}$$

where ρ_0 and p_0 are the liquid density and pressure reference, p is in Pascals and α_l and α_g are the liquid and gas sound velocities respectively.

Liquid Density Reference (kg.m^{-3})	1000
Liquid Pressure Reference (kg.m^{-3})	101325
Liquid Viscosity (cp)	50
Mud Rheology	Newtonian
Gas Viscosity (cp)	0.05
Water Sound Velocity (m.s^{-1})	1500
Gas Sound Velocity (m.s^{-1})	316

Table 5.13: *PVT Correlations used for Discontinuity Case and Udegbunam et al. (2015) Comparison*

5.2.1 Hypothetical Test Well - Single-Phase

For the hypothetical test well case, a hypothetical 9842 ft well (3000 m) is used with 5 distinct annulus regions. Table 5.15 shows the drilling schedule whereas Figure 5.1 shows a schematic of the described well profile. Table 5.14 shows the case information for the single-phase simulation:

Well Depth (ft)	9842.52
Pump Rate (gpm)	800

Table 5.14: *Input Parameters for Hypothetical Well Single-Phase Case*

Section	Casing Inner Diameter (in)	Drillstring Outer Diameter (in)	Section Length (ft)
1	20	6	1771.65
2	12	6	1574.8
3	12	5	3346.45
4	8	5	1574.8
5	8	4	1574.8

Table 5.15: *Hypothetical Well Drilling Schedule*

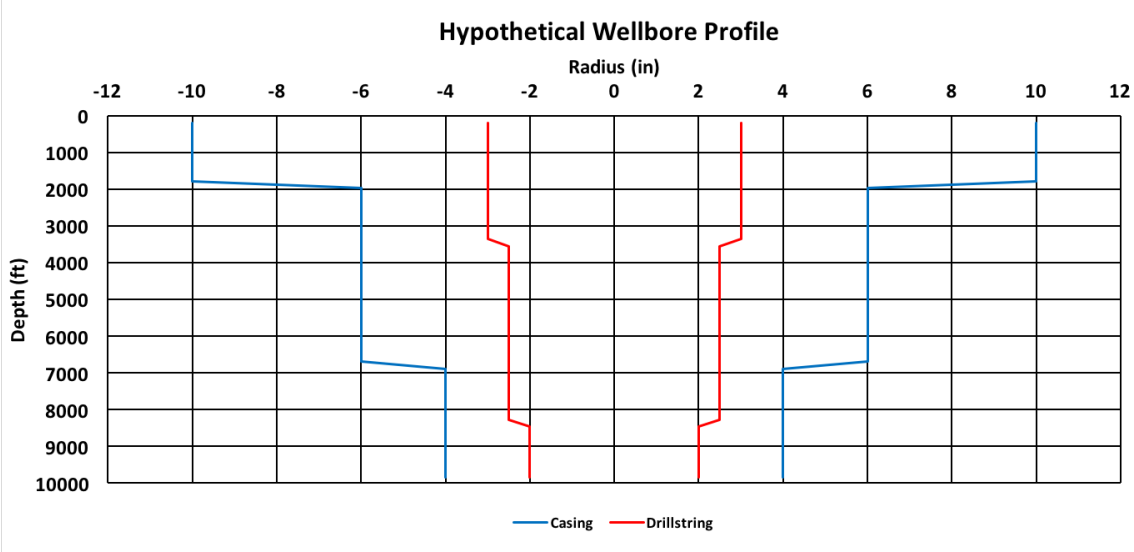

Figure 5.1: *Well Profile and Schedule of Test Well*

To verify the simulation, the steady state velocity profile is examined. The results for UTWELL are verified with the analytical solution for an incompressible liquid. Comparison between the UTWELL and analytical results along the wellbore are shown in Figure 5.2. The simulated BHP is shown in Figure 5.3. Comparison between the UTWELL results and the analytic solution for pressure is shown in Table 5.16 along with the percentage error.

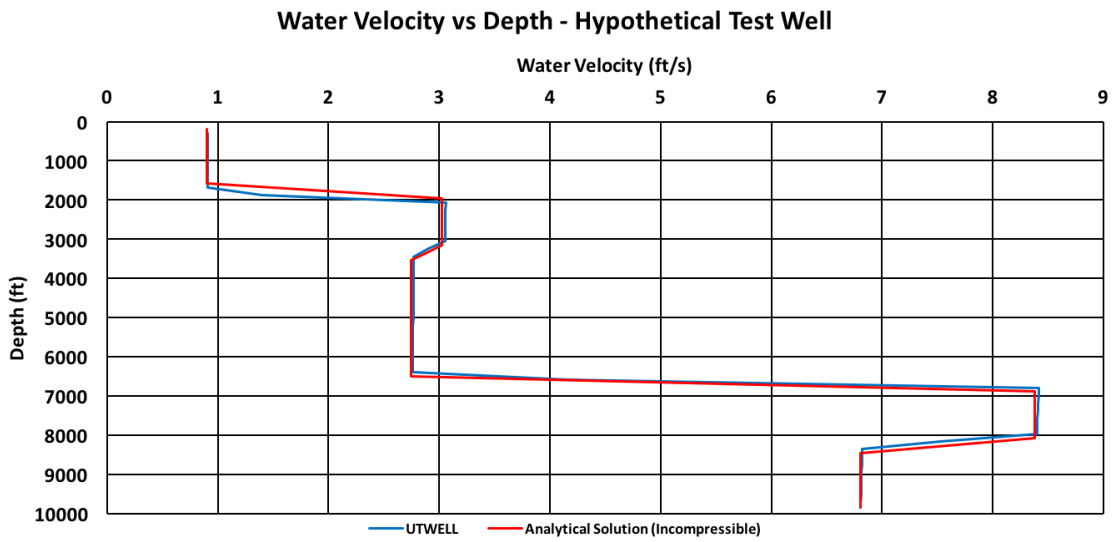

Figure 5.2: *Comparison of UTWELL Solution vs. Incompressible Analytical Solution for Steady State Flow With Discontinuities*

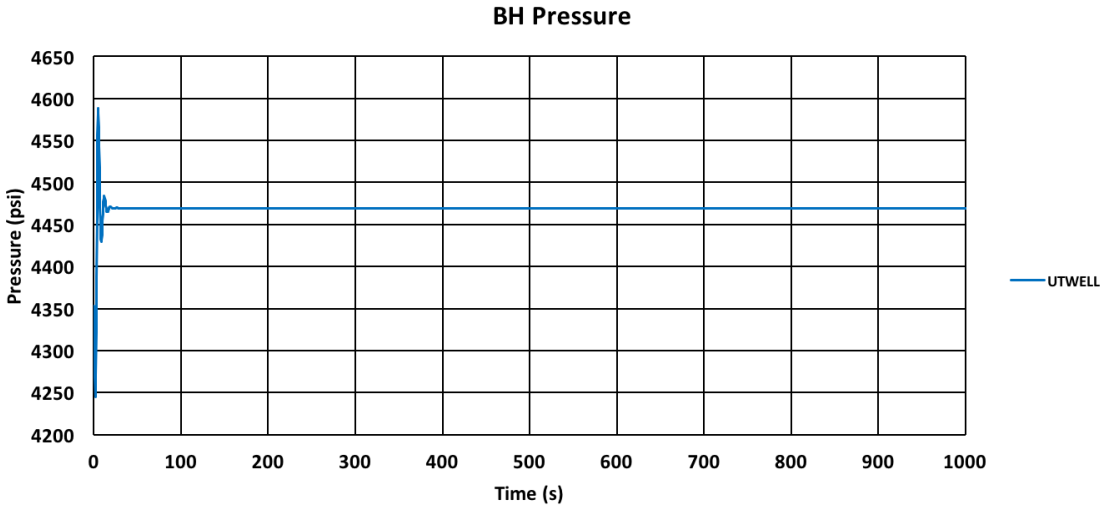

Figure 5.3: *Comparison of UTWELL Solution vs. Incompressible Analytical Solution for Steady State Flow With Discontinuities*

ΔP (psi)	Result	Percentage Error
Analytical	4464	-
Compressible Simulation	4470	0.134

Table 5.16: *Pressure Difference Results for Hypothetical Test Well single-phase Pipe Flow Simulation*

As can be seen, the results produced by UTWELL have strong agreement with the analytical solution for incompressible flow, for both velocity and BHP calculation. Any slight discrepancies could be due to numerical error, however, overall the results show that UTWELL is capable of handling discontinuities within the wellbore with reasonable accuracy. The simulated BHP was also matched the analytical solution. The reason as to why the percentage error for this case is lower than those seen in Section 5.1 could be due to the density correlation. Whilst in the previous simulations we incorporated the effects of temperature, the density correlation from Eq 5.1 is independent of temperature. This highlights the slight differences in results caused by correlations. In summary, UTWELL seems to be capable of accurately handling discontinuities for single-phase cases based on these results.

5.2.2 Hypothetical Test Well - Udegbunam et al. (2015) Multiphase Comparison

In order to verify the UTWELL multiphase models for drilling applications, a comparison is made with the MPD study presented by Udegbunam et al. (2015). In their simulation, they attempt to model the 'Floating Mud Cap' MPD model described by Fossli and Sangesland (2004), as well as Falk et al. (2011). In this method, the BHP is controlled by raising or lowering the hydrostatic column in the riser. This is done by pumping drilling mud through the drillstring, and then having an outflow at the bottom of the riser in order to either lower, maintain or increase the hydrostatic column in the riser.

Sequence of Events

Since UTWELL cannot perform the drainage function required to simulate the initial lowering of the level of the drilling mud, we instead modelled a well with a smaller riser to mimic the conditions from the Udegbunam et al. (2015) simulation prior to the introduction of the

gas kick. A fixed 0.5 m^3 (3.14 bbl) kick, measured at atmospheric conditions, is introduced at $t = 100$ seconds for a period 70 seconds. Drilling mud is then circulated at a rate of 600 $L.min^{-1}$ at $t = 200$ seconds. The sequence of events, and case parameters, are summarized in Table 5.17 whilst the he geometry of the wellbore is given in Table 5.18.

Start of Kick (s)	100
Kick Duration (s)	70
Start of Recirculation (s)	200
Recirculation Rate ($m^3.s^{-1}$)	0.06
Pit Gain Detection (m^3)	0.5

Table 5.17: *Case Parameters for Udegbunam et al. (2015) Comparison*

Section	Casing/Riser Inner Diameter (in)	Drillstring Outer Diameter (in)	Section Length (ft)
1	20	5	2690.29
2	8.5	5	3280.84

Table 5.18: *UTWELL Drilling Schedule of Udegbunam et al. (2015) Hypotethical Case Comparison*

For these simulations, Udegbunam et al. (2015) set the drift flux parameter as the following:

Drift Flux Parameter	Value
C_0	1.1
V_d^{gl} ($m.s^{-1}$)	0.5

Table 5.19: *Fixed Drift Flux Parameter Values as per Udegbunam et al. (2015)*

Figure 5.4 shows the BHP variation with time whilst Figures 5.5 through 5.8 show the variation of gas holdup throughout the wellbore.

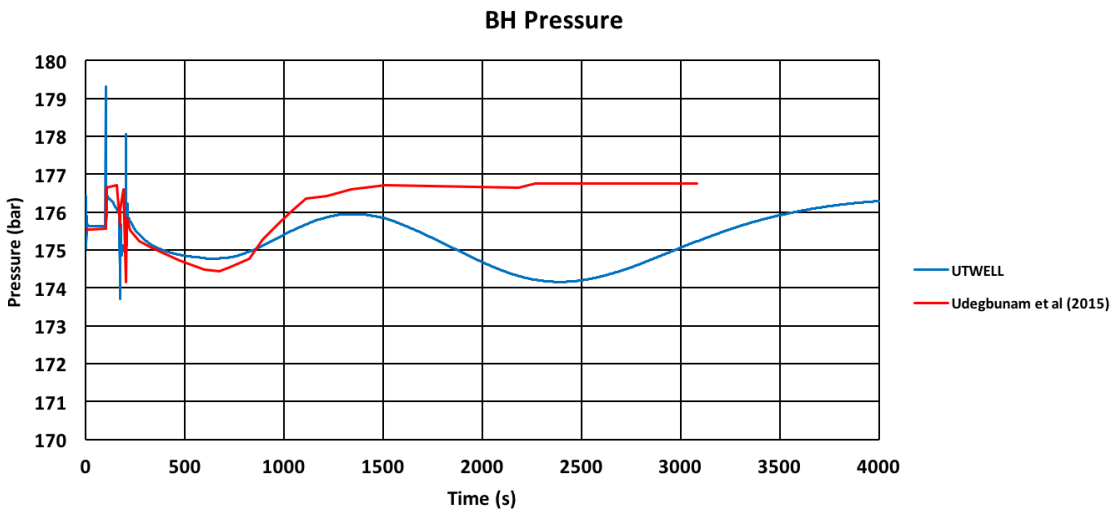

Figure 5.4: *Comparison of BHP Between UTWELL and Udegbunam et al. (2015)*

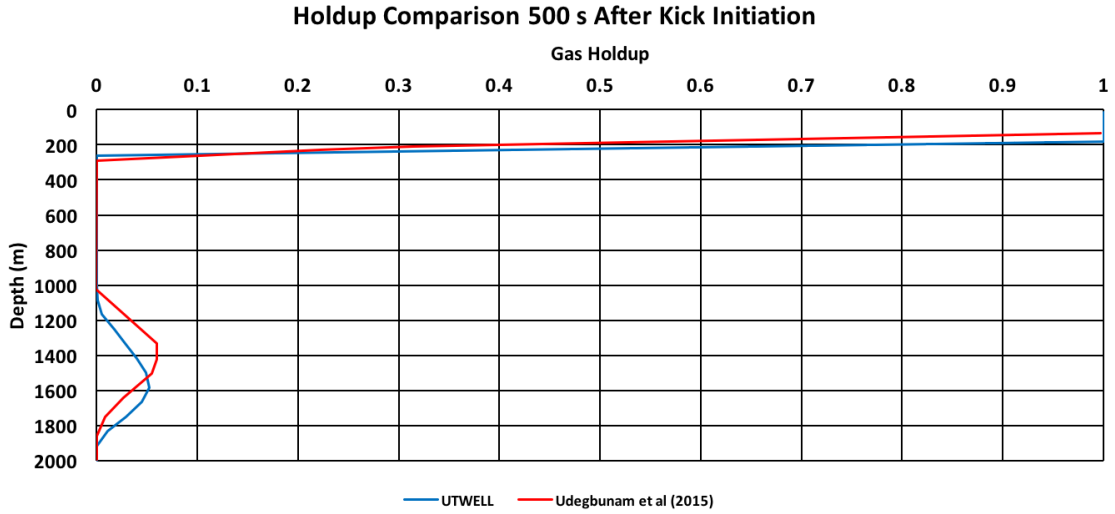

Figure 5.5: *Comparison of UTWELL holdup solution vs. Udegbunam et al. (2015) at 500s*

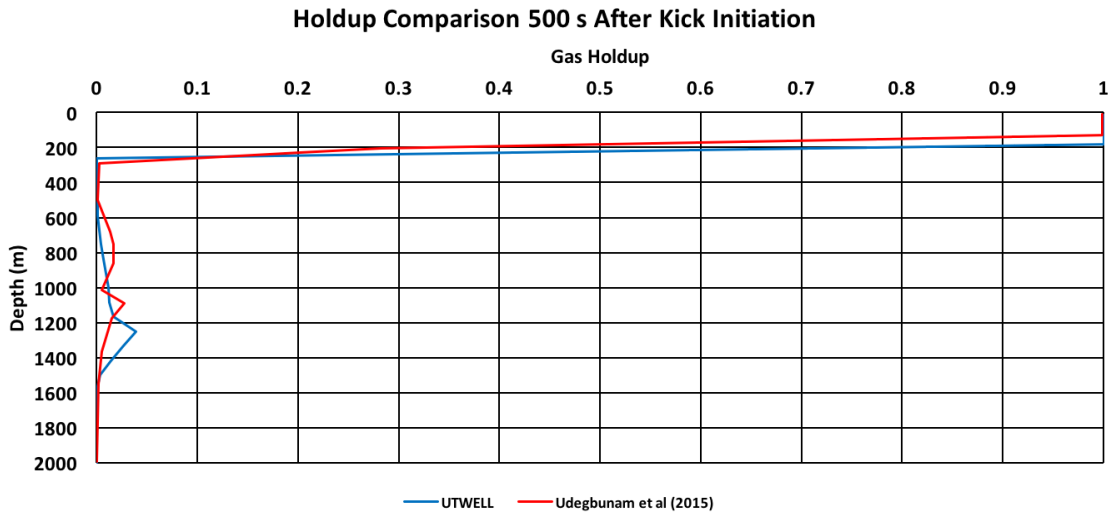

Figure 5.6: *Comparison of UTWELL holdup solution vs. Udegbunam et al. (2015) at 1000s*

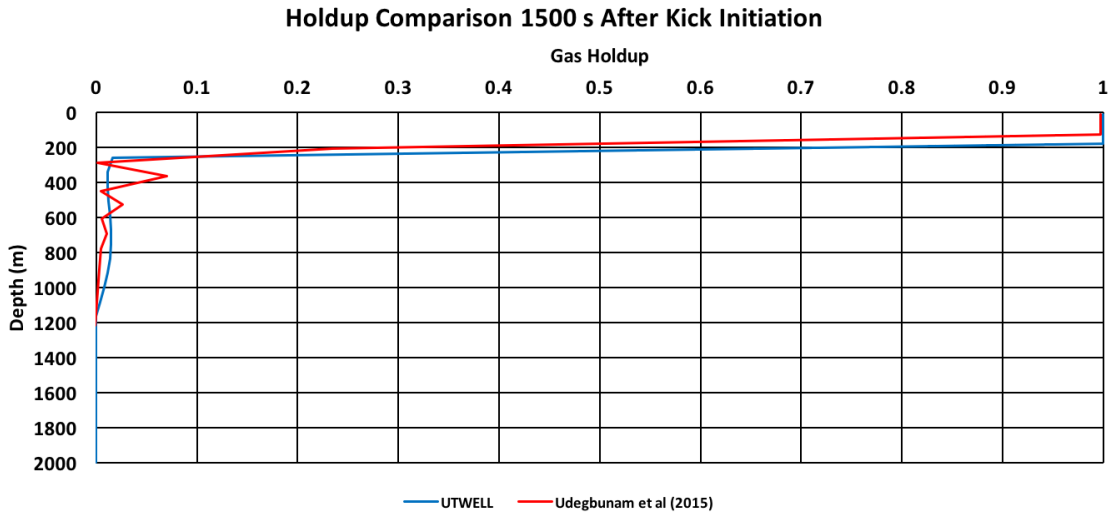

Figure 5.7: *Comparison of UTWELL holdup solution vs. Udegbunam et al. (2015) at 1500s*

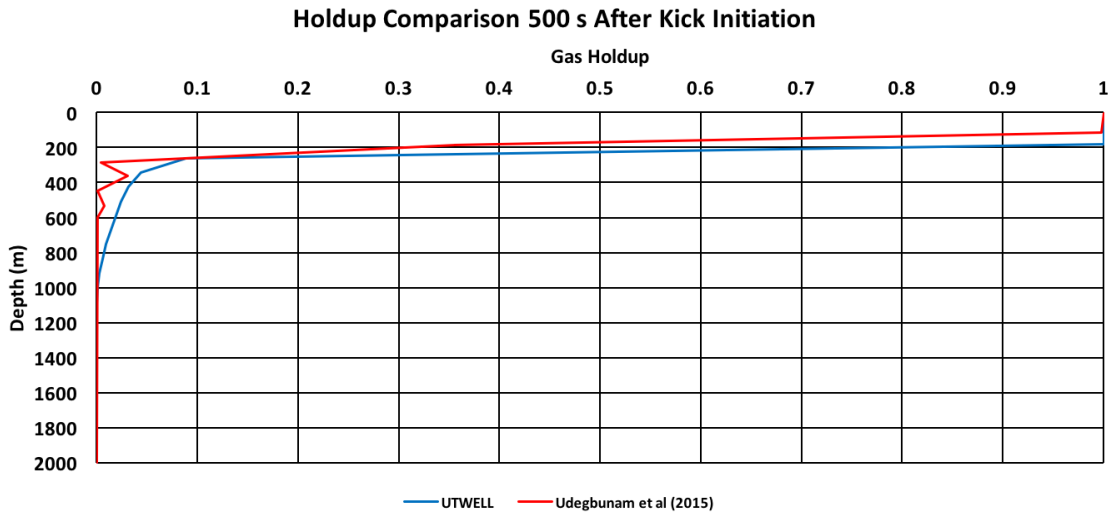

Figure 5.8: *Comparison of UTWELL holdup solution vs. Udegbunam et al. (2015) at 2100s*

It seems that UTWELL was unable to fully replicate the MPD procedure. The results had acceptable agreement until approximately 1300 seconds, which corresponds to the time at which the kick reaches the surface. Prior to that, it can be seen that UTWELL captured the onset of the gas kick with similar behaviour to that of Udegbunam et al. (2015).

Unlike UTWELL, the code developed by Udegbunam incorporates an Advection-Upstream-Splitting Method (AUSM) that better handles the pressure fluxes caused by discontinuities or shock waves. This is not the case in UTWELL, hence the reason for the higher oscillations when the kick is introduced, and at the start of recirculations. However, they both experience similar drops in pressure after the onset of circulation and experience very similar behaviour until approximately 800s. Udegbunam et al's simulation then sees a faster rise in BHP, which could be due to faster movement of the kick along the wellbore.

As shown in Figures 5.5 through 5.8, despite showing very similar behaviour, the gas bubble in theUdegbunam et al. (2015) simulation appears to be rising at a slightly higher velocity. This could be due to the different numerical scheme used. However, the difference does not seem to be significant as the gas holdup profile along the wellbore for both simulators seem to be very similar at the measured times.

The oscillation in the BHP seen in the UTWELL simulation is a physical event and not numerical error. The reason for the initial rise in pressure between the troughs in the UTWELL solution is caused by the discontinuity in the well. Since the riser has a bigger diameter than the casing, the gas kick bubble occupies less volume as it transitions into the riser. Thus, the vertical length occupied by the gas kick decreases, leading to an increase in BHP. An explanation for the second BHP drop could be due to the sudden expansion of gas at the surface. Prior to reaching the surface, the bubble travelled in a compressed state with pressure similar to that of the kick pressure. Once it reaches the surface, it has to come to equilibrium with atmospheric conditions. Thus, since pressure decreases, volume has to increase in order to compensate for this loss. Thus, more volume of gas is present in the wellbore, leading to a drop in BHP.

In order to test this hypothesis, the case was run with a constant diameter wellbore of $5.5''$ and $20''$. The Udegbunam et al. (2015) was also ran with non constant Drift Flux parameters to determine the effects of the assumption on the solution. It was also done to ensure that the troughs were not being caused by forced convergence of having set the slip velocity to be constant. In theory, if the well had a continuous diameter, only one trough would be present corresponding to the gas kick reaching the surface. Additionally, the solution of the well with variable diameter would be between the $5.5''$ and $20''$ constant diameter cases.The simulation results are shown in Figure 5.9.

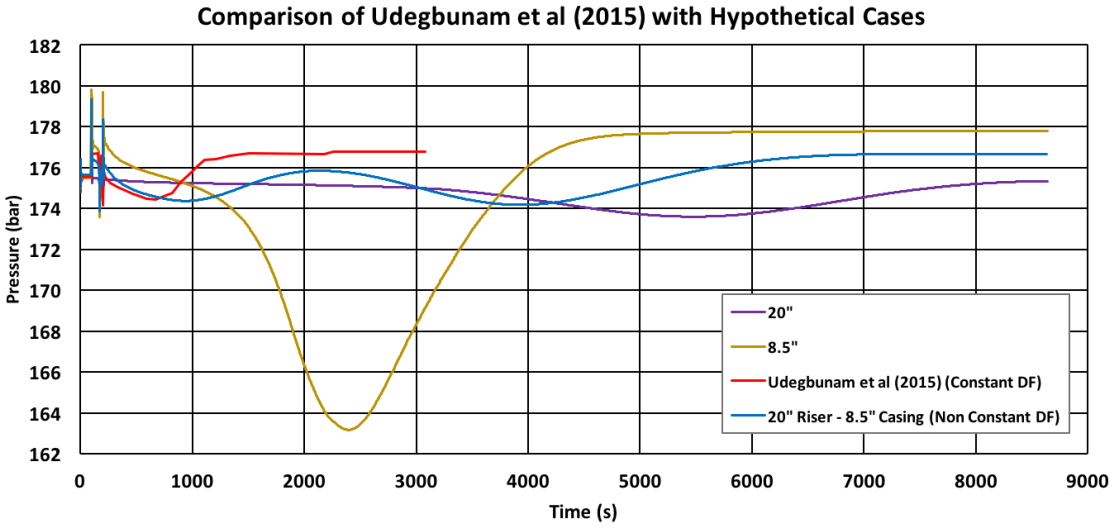

Figure 5.9: *Comparison of Various Hypothetical Wells to Verify Existence of Troughs*

As can be seen, there is only one trough present in both constant diameter cases, whilst there are still two troughs in the variable diameter case. Furthermore, the steady state BHP solution for variable diameter case lies between the steady state solution of the constant diameter simulations, as was predicted. The effect of having set the drift flux parameters can also be seen, as the non constant Drift Flux cases took much longer to reach steady state after flushing out the gas kick. The $5.5''$ Casing had the lowest drop in BHP due to the gas kick, since the gas bubble will occupy a larger portion of the hydrostatic column due to the smaller annular volume available. Additionally, it also had the highest steady state BHP solution. This is expected, as shown in the following derivations:

$$N_{Re} = \frac{\rho u D}{\mu} = \frac{\rho D}{\mu}\frac{4Q}{\pi D^2} = \frac{4\rho Q}{\pi \mu D} \tag{5.3}$$

$$f \propto \frac{1}{N_{Re}} \therefore f \propto D \tag{5.4}$$

$$\frac{dP}{dL} = f\frac{\rho u^2}{D} = f\frac{\rho}{D}(\frac{4Q}{\pi D^2})^2 = (D)\frac{16\rho Q^2}{\pi D^3} = \frac{16\rho Q^2}{\pi D^2} \tag{5.5}$$

Thus, higher diameters lead to an overall smaller pressure loss due to friction. This shows that UTWELL is producing results that obey the related physical phenomena, however it cannot handle this specific MPD technique. In the Udegbunam simulation, the

second trough was overcome by increasing the height of the mud column in the riser, as would be done in a floating mud cap system. As the kick is circulated out, the riser would be drained in order to maintain a constant mud height.

Since UTWELL cannot perform such a function, the method of MPD could not be accurately simulated. However, to confirm this hypothesis, a rough calculation was done which assumed that as soon as gas reached the surface, it would be replaced by water. This was done in order to simulate keeping the mud height constant, hence maintaining the hydrostatic pressure. Figure 5.10 shows the modified results. As can be seen, the results shows better convergence to the solution achieved by Udegbunam et al. (2015). A slight dip is still noticeable just after breakthrough, since at this time most of the gas bubble would still be inside the wellbore, but the solution converges to the same steady state solution as more gas reaches the surface.

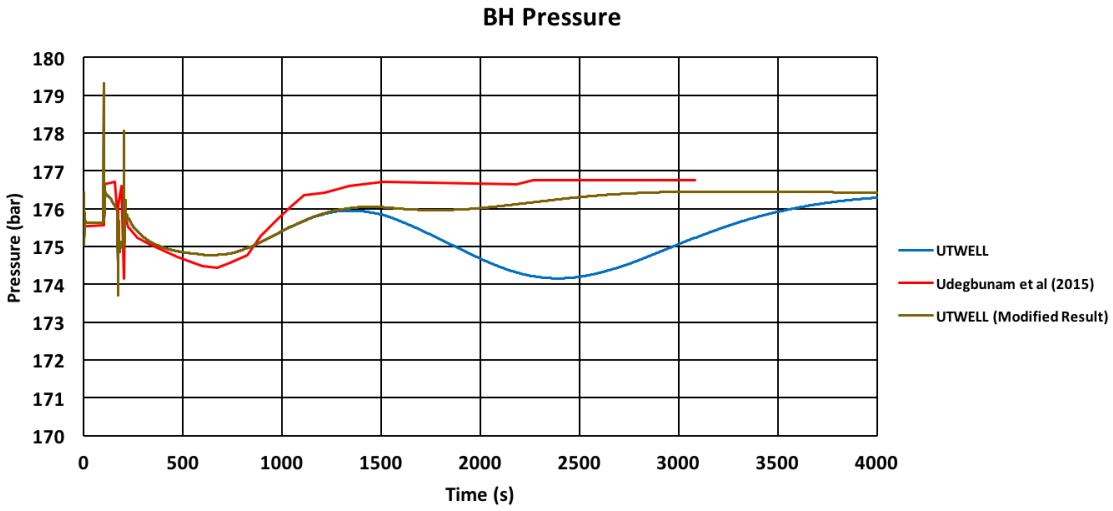

Figure 5.10: *Comparison of BHP Between UTWELL with modified results, and Udegbunam et al*

Albeit not fully successful since UTWELL could not fully simulate the MPD method, the fact that there was good match between UTWELL and the Udegbunam et al. (2015) simulation in capturing the pressure trend and movement of the kick prior to reaching the surface shows the capacity of UTWELL to handle multiphase flows even in wells with discontinuities.

5.3 Marques (2004) Kick Cases

In this section we compare UTWELL with the gas kick cases performed by Marques (2004). In order to obtain as accurate results as possible, we use the drilling mud fannmeter readings (Table 5.20) in order to determine the rheology parameters for the different rheology models, calculated using the guidelines suggested by Bourgoyne Jr et al. (1985).

Shear Rate	Readings
Θ_{600}	47
Θ_{300}	39
Θ_{200}	34
Θ_{100}	29
Θ_{6}	18
Θ_{3}	15

Table 5.20: *Fannometer Results from Marques (2004)*

Model	Rheological Parameters	
Newtonian	μ (cP)	28
Bingham	τ_y (lbf.100sqft^{-1})	8
Plastic	μ_p (cP)	31
Power	K (eq cP)	3485
Law	n	0.265

Table 5.21: *Rheological Parameters for drilling mud*

The Marques cases represent various tests that can be used to simulate well control methods at different stages of drilling operations. Figure 5.11 shows the schematic of the well used in the Marques (2004) experiments. The well profile parameters are given in Table 5.22 whilst Table 5.23 lists the sizes of the relevant connections. The gas kick is simulated through an injection line at the bottom of the well.

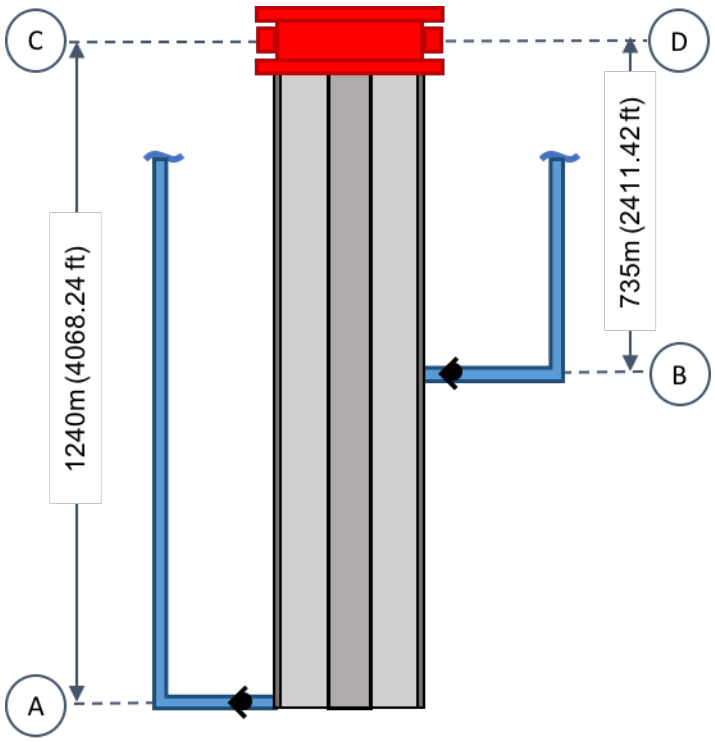

Figure 5.11: *Schematic of Wellbore Configuration for Marques (2004)*

Component	Length(m)	Diameter (in)
Casing	1240	6.18
Drillstring	1240	3.5
Submarine Choke Line	735	2

Table 5.22: *Test Well Profile from Marques (2004)*

Name	Connection	Internal Diameter (in)
Gas Kick Injection	A	0.85
Underground Choke	B	2
Surface Injection Line	C	3
Surface Choke Line	D	3

Table 5.23: *Relevant Connection parameters for Marques (2004) Well*

5.3.1 Onshore: No Drillstring Scenario

This scenario can represent a situation at which the drillstring has been fully removed from the wellbore. The wellbore can thus be modelled as a pipe with constant diameter, providing a good basis to test the multiphase correlations. Injection of liquid is given through the surface kill line whereas gas and liquid can only exit through the 3" surface choke line at the wellhead. This is illustrated in Figure 5.12.

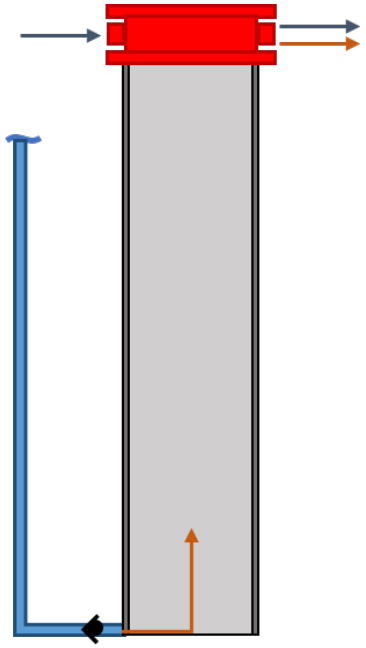

Figure 5.12: *Schematic of 'No Drillstring' Scenario*

Sequence of Events

The wellbore is initially filled with water and stationary. The gas kick is injected until a pit gain of 8 bbls is obtained. The well is then shut in. Once a pressure of 2400 psi is reached, drilling mud is then slowly injected from 0 to a rate of 85 gpm over a period of 120s at the surface in order to flush the gas kick. The sequence of events, and case parameters are shown in Tables 5.24 and 5.25. Figures 5.13 through 5.16 show the simulation results produced by UTWELL compared with the experimental data from Marques (2004).

Start of Kick (s)	300
Start of Recirculation (s)	2300
Recirculation Rate (gpm)	85
Pit Gain Detection (bbl)	8

Table 5.24: *Case Parameters for 'No Drillstring' Simulation*

Time (s)	Choke Percentage Opening (β_{open})
2300	0.15
2390	0.2
3250	0.205
4210	0.22
4950	0.21

Table 5.25: *Choke Opening Schedule During Recirculation for 'No Drillstring' Case*

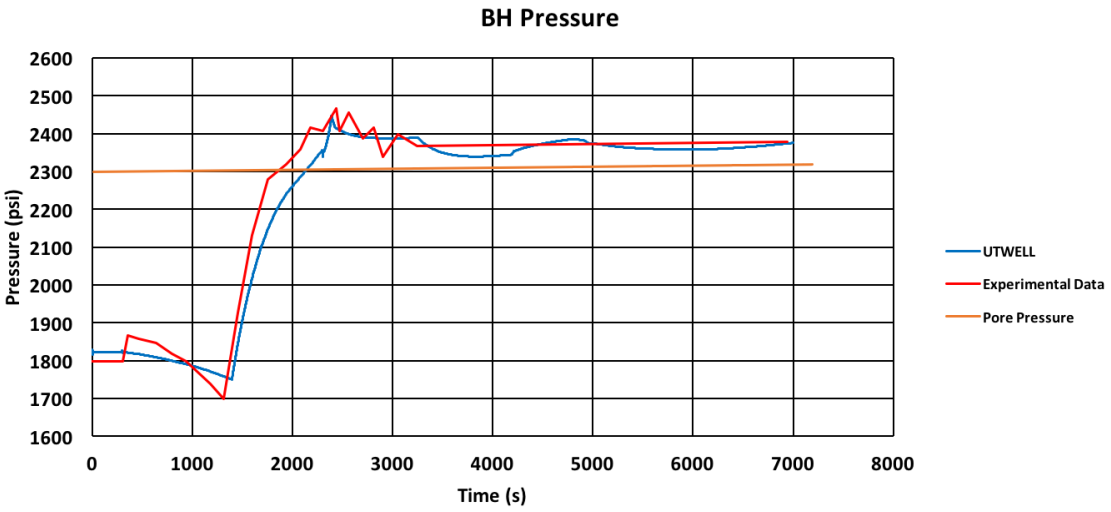

Figure 5.13: *BHP Results Compared With Experimental Data from Marques (2004) for 'No Drillstring' Case*

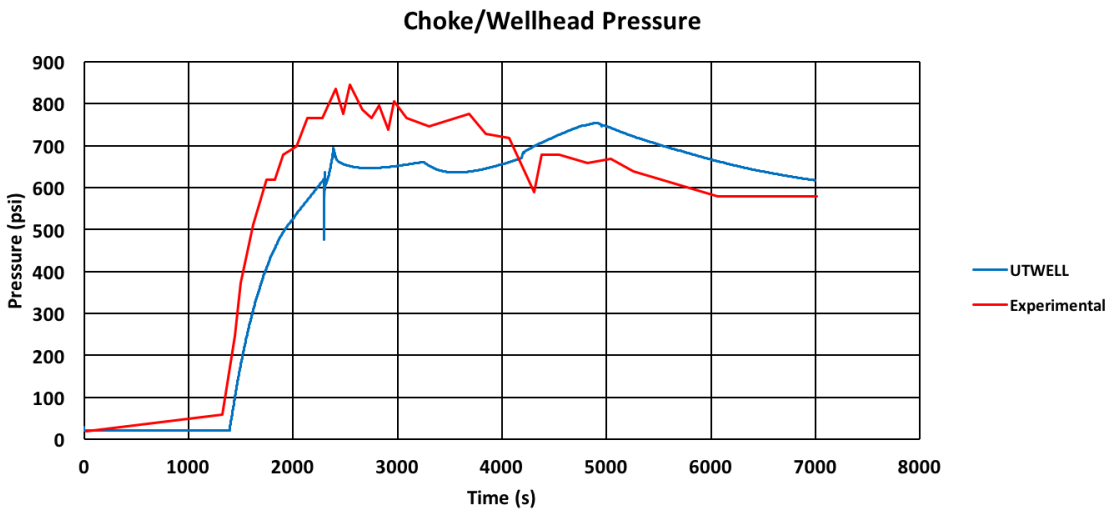

Figure 5.14: *Wellhead Pressure Results Compared with Experimental Data from Marques (2004) for 'No Drillstring' Case*

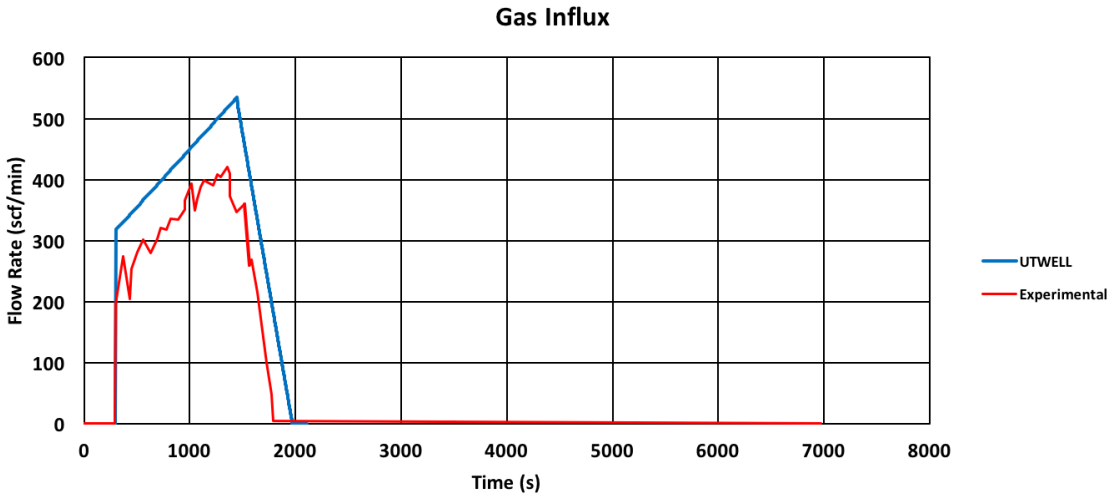

Figure 5.15: *Kick Influx Results Compared with Experimental Data from Marques (2004) for 'No Drillstring' Case*

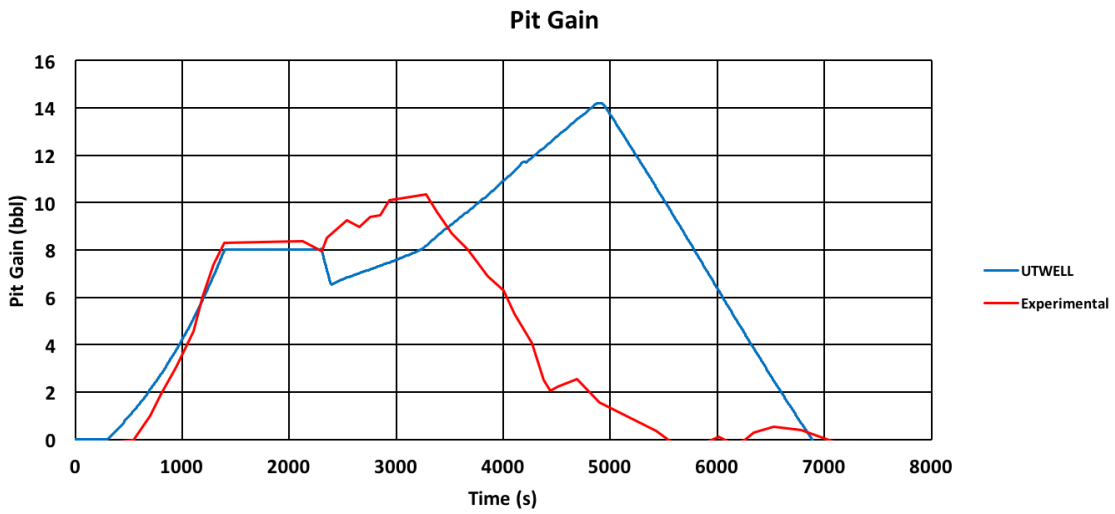

Figure 5.16: *Pit Gain Results Compared with Experimental Data from Marques (2004) for 'No Drillstring' Case*

The simulation produced a mixed set of results. Despite the BHP and choke behaviour presenting similar trends to the experimental results, both the Gas Influx and Pit Gain results have produced discrepancies. As seen in Figure 5.15, a larger influx of gas than that recorded by the experiment was required in order to produce a pit gain of 8 bbls at a similar time as the experiment.

The discrepancy in the Pit Gain (Figure 5.16) could be due to the gas bubble moving at a slower rate than in the experiment. Since the bubble in the simulation spends a longer time inside the wellbore, it is constantly expanding and hence pushing more mud out. Hence, there is a prolonged increase in Pit Gain in the simulation than during the experiment. The peak in the simulation Pit Gain at around 4800 seconds corresponds to the choke peak in Figure 5.14, the moment at which the gas bubble begins to exit the wellbore through the choke. Subsequently, the choke pressure rapidly decreases as the BHP is kept constant. In the experiment, the choke pressure begins to decrease at approximately 3500 seconds, which corresponds to the Pit Gain peak for the experimental data. Hence, the reason for the discrepancy could be caused by a delay in the movement of the bubble, similar to what was seen in Section 5.2.2. This could be fixed by careful calibration of the Drift Flux correlations. Despite this, the simulator seems to follow the general trends.

Another source of error for the discrepancy in the pit gain is the fact the surface gas flow rate for UTWELL was higher than the experimental data. If the compressibility of the simulated gas was higher than in the experiment, more gas would be required in order to displace the same volume of drilling mud. Thus, more gas enters the wellbore, and consequently more will have to be flushed out of the wellbore. Thus the discrepancy represents the additional volume of gas that had to be removed from the wellbore.

5.3.2 Onshore: Drillstring up to 490m

This scenario resembles that of a tripping situation where the drillstring is being removed during the onset of the kick. The return of liquid occurs at the surface choke line whereas the injection of liquid occurs at the drillstring.This is illustrated in Figure 5.17.

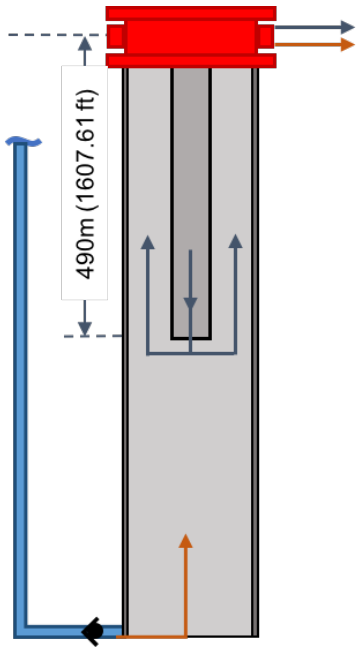

Figure 5.17: *Schematic of 'Semi Submerged Drillstring' Scenario*

Sequence of Events

The drillstring is positioned 490m below the surface. Thus, the geometry can be modelled as a pipe followed by an annular geometry. The wellbore is initially filled with water based drilling mud and stationary. The gas kick is injected from the bottom of the wellbore. After a pit gain of 8bbl is recorded, the well is shut in. Once the BHP has reached a pressure

of 2300 psi, drilling mud is recirculated through the drillstring into the wellbore. The kick is circulated out at a rate of 85gpm. The sequence of events, and case parameters are shown in Tables 5.26 and 5.27. Figures 5.18 to 5.21 show the simulation results produced by UTWELL compared with the experimental data from Marques (2004).

Start of Kick (s)	310
Start of Recirculation (s)	2300
Recirculation Rate (gpm)	85
Pit Gain Detection (bbl)	8

Table 5.26: *Case Parameters for 'Semi Submerged Drillstring' Case*

Time (s)	Choke Percentage Opening (β_{open})
2300	0.21
4000	0.22
5200	0.215
6700	0.22
8550	0.2075

Table 5.27: *Choke Opening Schedule During Recirculation for 'Semi Submerged Drillstring' Case*

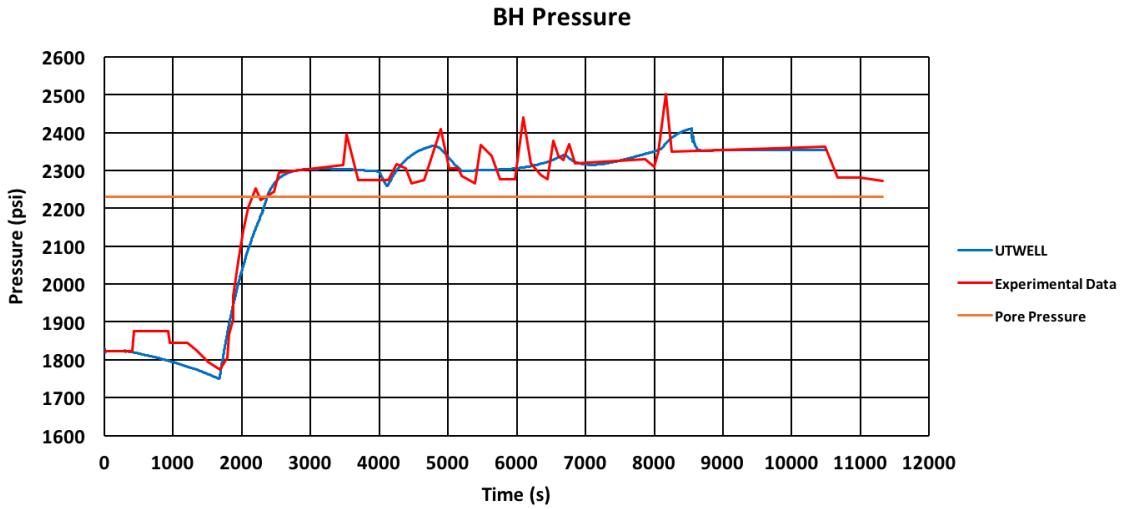

Figure 5.18: *BHP Results Compared With Experimental Data from Marques (2004) for 'Semi Submerged Drillstring' Case*

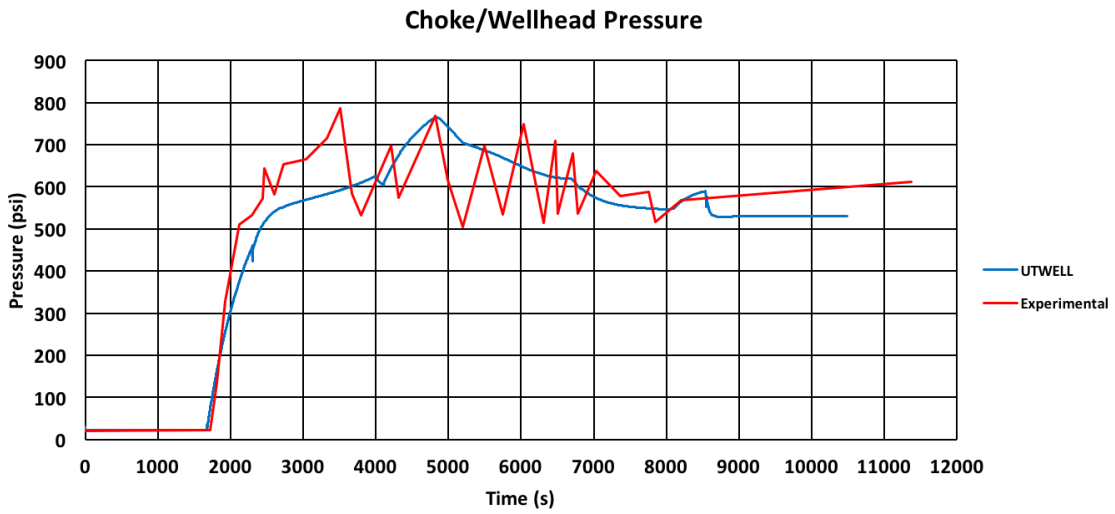

Figure 5.19: *Wellhead Pressure Results Compared with Experimental Data from Marques (2004) for 'Semi Submerged Drillstring' Case*

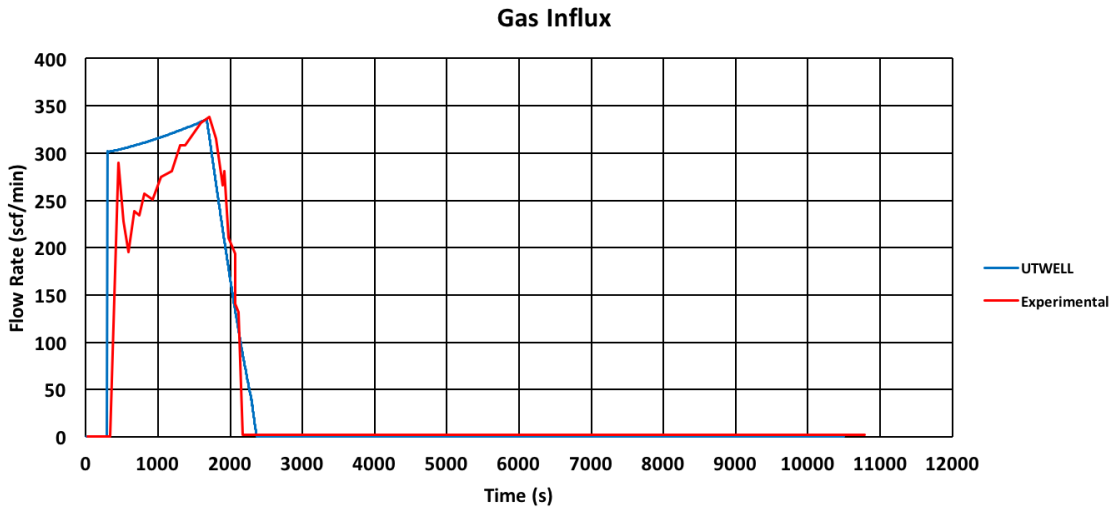

Figure 5.20: *Kick Influx Results Compared with Experimental Data from Marques (2004) for 'Semi Submerged Drillstring' Case*

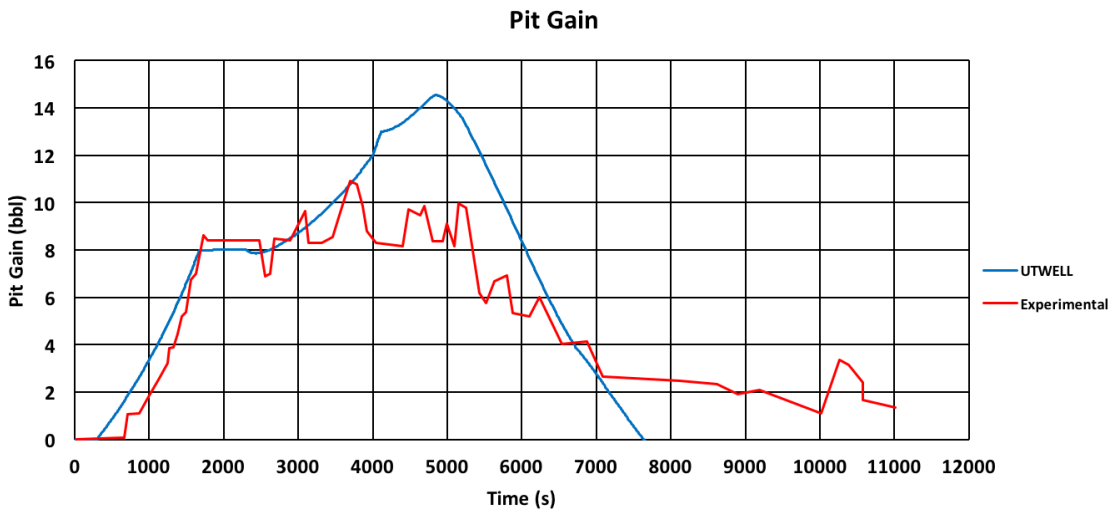

Figure 5.21: *Pit Gain Results Compared with Experimental Data from Marques (2004) for 'Semi Submerged Drillstring' Case*

Similar to the previous case, the BHP and Choke simulation results have good agreement with the experimental data. Furthermore, the Gas Influx has a better correlation, however the pit gain once again produced discrepancies during the recirculation stage. The maximum pit gain was greater than the peak seen in the experimental results, however the Pit Gain decreased to a value of zero earlier than in the experiment, meaning the kick was flushed out at a quicker rate.

It was noticed that the general shape of the Pit Gain in Figure 5.21 is similar to the one seen in Figure 5.16. This could mean that the reason for the discrepancies in both cases could be a systematic error in the the boundary conditions during the recirculation stage for the purpose of calculating the pit gain. This could either be a modelling error, or also be a lack of data from Marques where a certain action was being performed during the experiment that was not discussed in their report.

Despite the discrepancy, the consistency in the BHP, Choke and Gas Influx data with the experimental results suggest that UTWELL is capable of handling gas kick cases.

5.3.3 Offshore: Drillstring at the Bottom Scenario

This scenario represents a normal drilling situation at an offshore well water depth of 740 m. The column is modelled as initially being an annulus. However, once the choke depth is reached, pipe flow is modelled. The return of fluid occurs through the choke line whilst the injection of liquid is performed through the drillstring. This is illustrated in Figure 5.22.

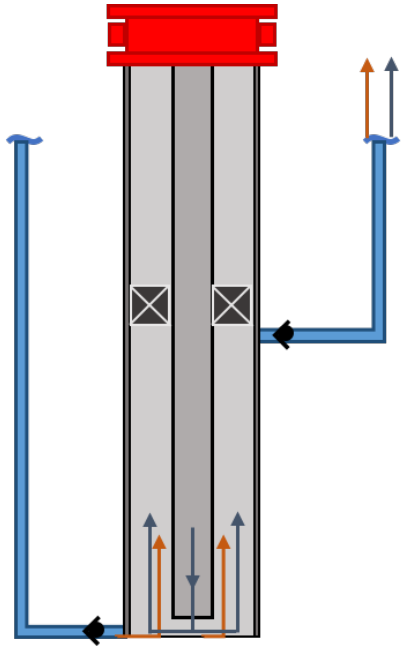

Figure 5.22: *Schematic of 'Offshore' Scenario*

Sequence of Events

No mud is initially circulated. A gas kick is then introduced in the wellbore, displacing the mud. After a pit gain of 4 barrels has been detected, the well is shut off and the gas kick allowed to migrate. The pressure in the wellbore slowly increases and until a pressure of 2100 psi is reached. Mud is then recirculated at a rate of 42 gpm. As the kick nears the surface, the choke is adjusted to ensure that the BHP remains at approximately 2100. The sequence of events, and case parameters, are shown in Table 5.28 whilst the choke schedule during recirculation is shown in Table 5.29. Figures 5.23 through 5.27 show the simulation results produced by UTWELL compared with the experimental data from Marques (2004) and Avelar (2008).

Start of Kick (s)	140
Start of Recirculation (s)	1640
Recirculation Rate (gpm)	42
Pit Gain Detection (bbl)	4

Table 5.28: *Case Parameters for Offshore Simulation*

Time (s)	Choke Percentage Opening (β_{open})	Time (s)	Percentage Opening (β_{open})
1640	0.25	2280	0.28
1685	0.33	3060	0.3
1770	0.3	3300	0.32
1940	0.34	3890	0.3
2060	0.32	4210	0.297

Table 5.29: *Choke Opening Schedule During Recirculation*

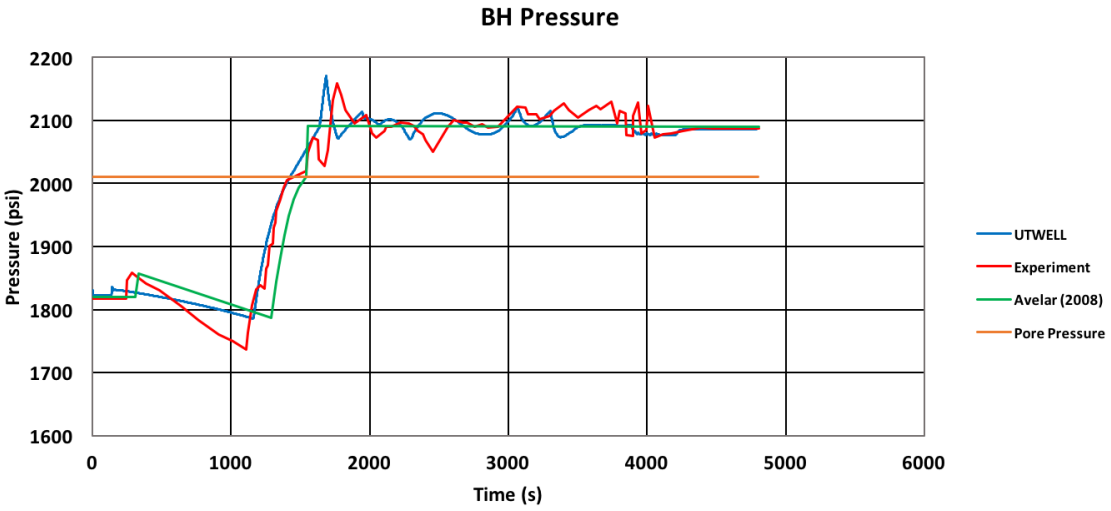

Figure 5.23: *BHP Results Compared With Experimental Data and Avelar Simulator*

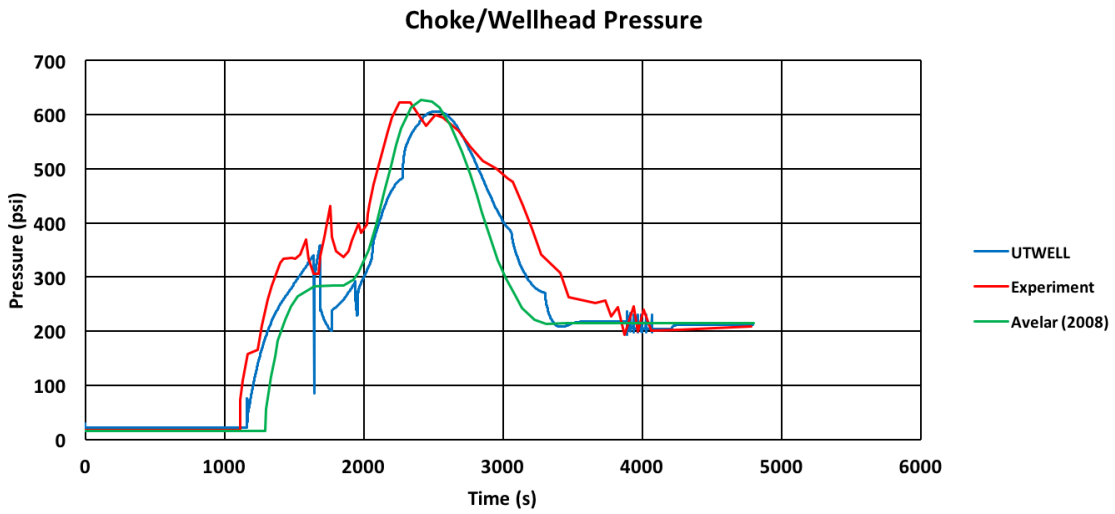

Figure 5.24: *Wellhead Pressure Results Compared with Experimental Data from Marques (2004) and Avelar et al. (2008, 2009) Simulator*

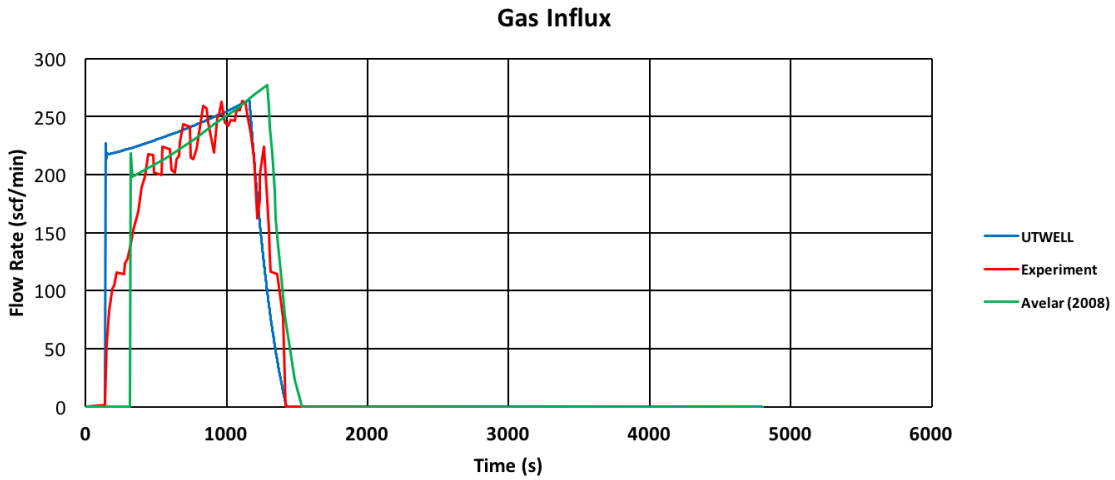

Figure 5.25: *Kick Influx Results Compared with Experimental Data from Marques (2004) and Avelar et al. (2008, 2009) Simulator*

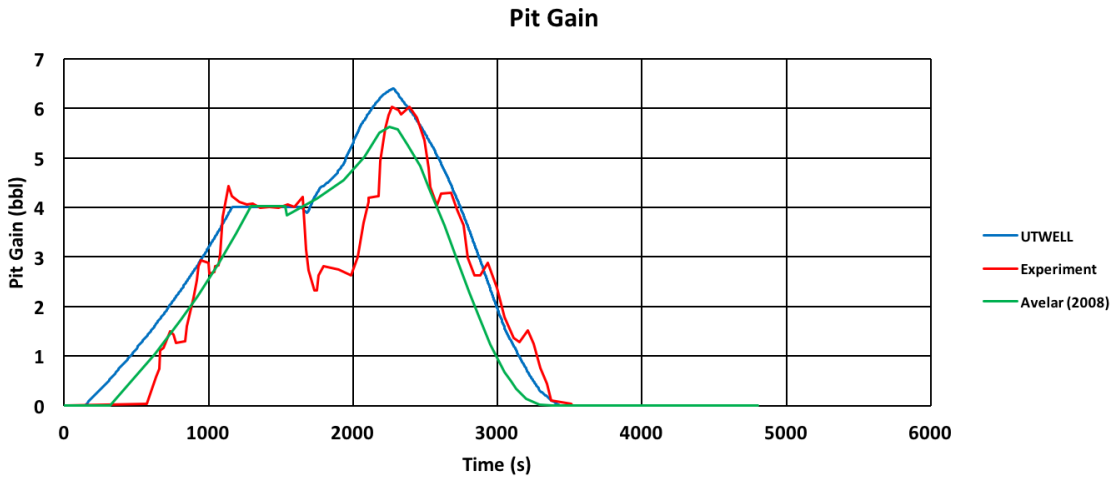

Figure 5.26: *Pit Gain Results Compared with Experimental Datarom Marques (2004) and Avelar et al. (2008, 2009) Simulator*

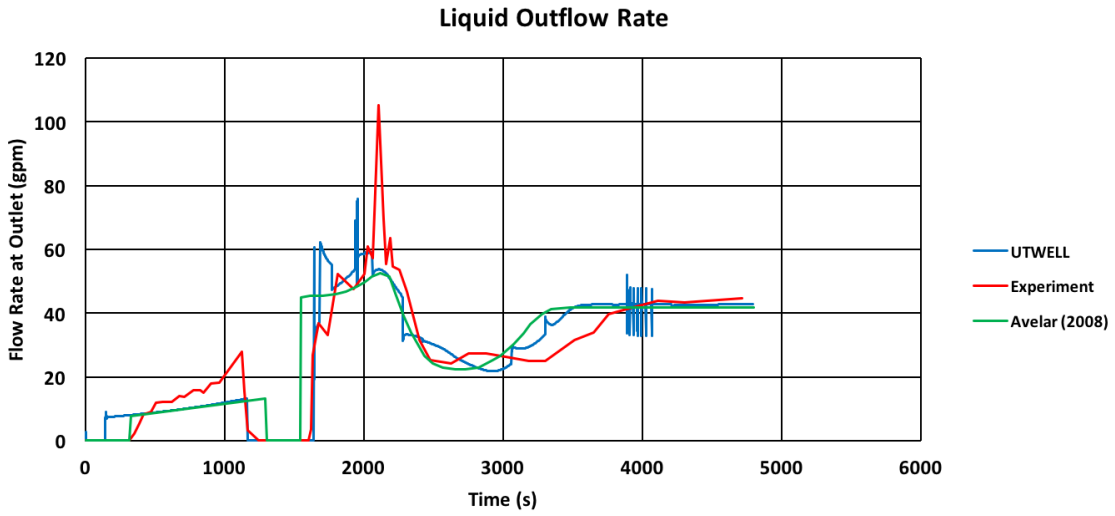

Figure 5.27: *Mud Outflow Rate Results Compared with Experimental Data from Marques (2004) and Avelar et al. (2008, 2009) Simulator*

The trends produced by UTWELL are in good agreement with the Marques (2004) and Avelar (2008) results. There are a few discrepancies, however. In Figure 5.23 it can be seen that at time of shut in, the BHP does not decrease to the same level as the experimental data, however it is consistent with the Avelar simulation. This is in contrast to Figures 5.13 and 5.18 where the decrease in pressure caused by the kick matched the experimental

data.

The onset of the kick in UTWELL appears to have an immediate effect on the simulation data, an effect seen in the previous simulations as well. Despite the kick being initiated at the same time as the experimental results, there seems to be a delayed response in the experimental data. In the experimental trial, the increase in pit gain, mud outflow and BHP hike occur well after the onset of the kick. In UTWELL, these events occur simultaneously with the onset of the kick. In Figure 5.23 it can be seen that the BHP hike occurs before the experimental and Avelar results. The same phenomenon is seen in Figure 5.27 where the increase in outflow of mud happens much earlier than in the Avelar or experimental data. Likewise, the increase in Pit Gain in Figure 5.26 starts at the same time the kick begins. This appears to be a numerical effect, as the same thing is seen in the Avelar results where increases in BHP, Pit Gain and mud outflow are also simultaneous with the onset of the kick in their simulation. The reason they occur later because the kick is initiated at a later time.

There is a slight overshoot in the Pit Gain simulation of UTWELL as seen in Figure 5.26. This could once again be related to the speed of the bubble being slower. Since the bubble takes slower to be flushed out of the well, it has more time to expand. This expansion, in turn, causes for a higher outflow rate. Figure 5.27 shows that at the same time the overshoot occurs in Figure 5.26, the outflow rate is higher than the experimental data, and hence the reason for the overshoot. Conversely, the overshoot could also be due to the higher influx of gas in UTWELL than in the experimental data at the beggining of the kick. Another discrepancy noticed was that neither UTWELL and Avelar simulations were not able to accurately match the Pit Gain dip seen between 1800s - 2200s of the experimental results. This could once again suggest that an additional operation was carried out which led to the decrease in Pit Gain, only to then be followed by a large increase. The UTWELL pit gain trend since in Figure 5.26 matches the behaviour seen in the previous two cases.

Despite the mentioned discrepancies, the agreement in general trends and behaviour does show the potential of UTWELL to be an effective tool for gas kick simulation.

5.3.4 General Comments on the Marques Case Studies

Several patterns were noticed during the Marques case studies. First, the simulated BHP and Choke pressures in general had good agreement with the experimental data throughout all three cases. This means that the pressure profiles calculated by the SIMPHM algorithm are robust and UTWELL can be used for calculation of pressure data over time. It was also noticed that as the cases progressed, there seemed to be better agreement of the UTWELL simulations for both the gas influx into the wellbore and the recorded pit gain.

In all cases, there were visible discrepancies between the experimental pit gain and that simulated by UTWELL. In the 'No Drillstring Case', the maximum pit gain recorded by UTWELL was greater, and occurred at latter time, than the experimental case. However, by the end of the simulation, both UTWELL and the experiment had reached a pit gain of zero. In the Semi-Submerged Drill string case, UTWELL recorded a maximum pit gain that was higher than the experimental data, however the kick was also flushed out of the wellbore at an earlier time. In the Offshore case, there was a segment in the experiment where the pit gain dipped before rising again, however neither UTWELL nor Avelar's simulator were capable of mimicking this phenomenon, bringing the possibility that an additional procedure was performed by Marques which was not reported. Furthermore, it was observed that the general trend of the different pit gain graphs were similar to each other. This brought up the possibility that the discrepancies could also be caused by a systematic error in either the calculation of the pit gain, or the boundary conditions during recirculation.

Overall, it can be confirmed that UTWELL was able to simulate the different case studies, which represented different drilling operations, with reasonable accuracy. Although UTWELL has proven to be a robust simulator, further time should be devoted into examining the multiphase correlations, particularly friction factors and velocity correlations, as these could have had the biggest influence on the results.

Chapter 6

Conclusions and Recommendations

6.1 Summary and Conclusions

UTWELL was modified in order to include a gas kick simulator module for drilling applications. To accomplish this, tools were integrated to allow for the changing of boundary conditions during the simulation in order to mimic the different stages of a gas kick and its' control. Additionally, components such as a Pit Gain indicator and choke control were incorporated to model MPD via choke management. Several tests were then employed in order to test the robustness of the simulator:

- UTWELL simulations showed good agreement with analytical solutions for single-phase flows for different liquid rheologies. Furthermore, there was no discernible different between compressible and non compressible flow simulations, making non-compressible analytical solutions a good benchmark for additional tests.

- Wellbore geometries with discontinuities were tested to see if UTWELL was capable of handling them. Well discontinuities were a feature not commonly seen in literature, as most opt for single diameter cases. Results showed good agreement with the non compressible analytical solution for steady state flow. The analytical pressure drop was also consistent with the UTWELL simulation, confirming the capability of UTWELL to run simulations with variable wellbore geometries.

- UTWELL was compared with the simulator developed by Udegbunam et al. (2015) in order to test and compare the multiphase simulator. The results were mixed. Despite

UTWELL being able to capture the gas kick and movement of the kick along the wellbore with good agreement, it was not able to mimic the MPD strategy employed by Udegbunam et al. (2015) to maintain a constant BHP as the kick left the wellbore.

- Despite not being able to replicate the second half of the simulation, it was shown that UTWELL was still producing a physical and expected result. This, along with closely replicating the first half of the Udegbunam et al. (2015) simulation, confirmed UTWELL's robustness as a multiphase simulator.

- UTWELL was compared with three distinct cases taken from well tests from Marques (2004). All three simulations shows good agreement with the experimental data for BHP and choke trends.

- The 'No Drillstring' and 'Semi-Submerged Drillstring' showed large discrepancies with the pit gain simulations, in both cases showing significantly higher peak pit gains than the experimental results. Since the general behaviour for the pit gain was similar in all three simulations, there could be a systematic error in how the pit gain is calculated which could have led to these errors.

- Another discussed issue was that extra actions could have occurred during the well tests which affected the experimental data for pit gain. This was suggested when it was noticed that neither UTWELL nor the simulation results from Avelar (2008) were able to capture a pit gain dip seen in the final experimental case.

6.2 Future Recommendations

UTWELL in general was able to simulate both hypothetical and experimental cases with good tolerance. Thus, the simulator in its' current form provides an adequate base to be improved upon. The following are suggestions that could be the focus for future work:

- In this thesis, only water-based muds were tested, therefore there was no consideration of solubility effects between the gas kick and the mud. Inclusion of the capability to simulate oil-based muds, similar to the work of Loiola (2015) and Rommetveit and Vefring (1991), is desirable in order to study the effects of gas kicks in oil based mud. For this to occur, a compositional model with Equation of State, as opposed to the Blackoil method used in this Thesis, would have to be implemented for best accuracy.

- The choke control in this thesis was done manually, requiring mutliple runs in order to make sure that the pressure would be kept at a specific BHP. This took significant time and thus one suggestion would be to implement a control loop feature, similar to that seen in Ambrus et al. (2015), to make it automatic.

- Despite the various rheology models implemented, these only worked well during steady state single-phase and not for multiphase flow. This was attributed to the fact that the Beggs and Brill multiphase correlation are for Newtonian fluids whose apparent viscosities may not be as high as those seen in certain non newtonian fluids, particularly at low velocities. This high contrast between viscosities caused convergence problems. Research and inclusion of friction factor correlations for multiphase flow for non newtonian fluids could ameliorate this issue.

- Although there was a good agreement in the trends seen between UTWELL and the Udegbunam et al. (2015) simulator as the kick entered the wellbore, the oscillations were more severe in UTWELL. It would be desirable for UTWELL to be capable of better handling the pressure fluxes. It is recommended that the discretization is modified to include some of the flux splitting techniques seen in Udegbunam et al. (2015) and Fjelde and Karlsen (2002) to better handle the momentum and pressure fluxes across nodes.

- The reason that the 'Floating Mud Cap' MPD system was not simulated by UTWELL was due to the fact that it could not perform drainage operations. That is, it could not effectively simulate the decrease in liquid height, decrease in BHP and entry of air in a column of water that is drained. UTWELL should be modified to be capable of simulating such situations as they also occur in normal drilling operations, such as the drop in water level as the drillstring is pulled out during tripping operations.

- The effects of cuttings and other insoluble media have a massive effect on circulation and BHP management during drilling operations and, according to Costa, Da Fontoura, and Martins (2008), are one of the biggest causes for lost time events. Inclusion of cuttings would be beneficial to UTWELL and the numerical simulation of the phenomena is a field yet to be extensively researched.

Appendix A

Shi et al. (2005) Drift Flux Correlation

A.1 Gas/Liquid Parameters

Profile Parameter

The following represents the method described by Shi et al. (2005) for calculating the Drift Flux parameters of each respective phase. The gas phase velocity is defined as

$$u_g = C_0 + V_d^{gl} \tag{A.1}$$

where C_0, the profile parameter, is defined as

$$C_0 = \frac{A}{1 + (A-1)\gamma^2} \tag{A.2}$$

The parameter γ is given by

$$\gamma = \frac{\beta - B}{1 - B} \tag{A.3}$$

β is a parameter that tends to 1.0 as α_g tends to 1.0, and at high values of u_m. Thus, as $\alpha_g \to 1.0$, $C_0 \to 1.0$. β is defined as

$$\beta = \max\left(\alpha_g, F_v, \frac{\alpha_g |u_m|}{u_{sgf}}\right) \tag{A.4}$$

For Eqs A.1 through A.4, A, B and F_v are parameters that are tuned to fit observations. For all cases presented in this Thesis, the parameters are shown in Table A.1.

Parameter	Value
A	1.0
B	0.3
F_v	1.0

Table A.1: *Parameter Values for Drift Flux Calculations of Gas and Liquid*

Drift Velocity

The gas slip velocity is calculated as

$$V_d^{gl} = \frac{(1-\alpha_g C_0) C_0 K_{\alpha_g} V_c}{\alpha_g C_0 \sqrt{\frac{\rho_l}{\rho_g}} + 1 - \alpha_g C_0} \tag{A.5}$$

where

$$V_c = \left(\frac{\sigma_{gl} g (\rho_l - \rho_g)}{\rho_l^2} \right)^{1/4} \tag{A.6}$$

The parameter K_{α_g} is dependent on the gas holdup, α_g. If $\alpha_g \leq 0.2$:

$$K_{\alpha_g} = \frac{1.53}{C_0} \tag{A.7}$$

If $\alpha_g \geq 0.4$ (Ambrus et al., 2015):

$$K_{\alpha_g} = 3.182 \left(1 - e^{\frac{\hat{D}}{9.3833}} \right) \tag{A.8}$$

where

$$\hat{D} = \left(\frac{g(\rho_l - \rho_g}{\sigma_{gl}} \right)^{1/2} D \tag{A.9}$$

For α_g values between 0.2 and 0.4, linear interpolation is used. The definition of mixture velocity is

$$u_m = \alpha_g u_g + \alpha_l u_l = \alpha_g u_g + (1-\alpha_g) u_l \tag{A.10}$$

using the definition from Eq A.1, Eq A.10 can be rearranged to define u_l as

$$u_l = \frac{1 - \alpha_g C_0}{1 - \alpha_g} u_m + \frac{\alpha_g}{1 - \alpha_g} V_d^{gl} \tag{A.11}$$

A.2 Oil/Water Parameters

The procedure for calculating the water and oil drift flux coefficients mirrors that of the gas liquid coefficients. In this case, the liquid phase is defined as

$$u_l = \alpha_o u_o + \alpha_w u_w \tag{A.12}$$

, hence

$$u_o = C_0' u_l + V_d' \tag{A.13}$$

$$u_w = \frac{1 - \alpha_o C_0'}{1 - \alpha_o} u_l + \frac{\alpha_o}{1 - \alpha_o} V_d' \tag{A.14}$$

To determine the coefficient C_0^{ow} and V_d^{ow}, Shi et al. refer to the work of Hasan and Kabir (1998).

Profile Parameter

To determine C_0', Hasan and Kabir (1998) suggest the following criterion:

$$C_0' = A', \alpha_o \leq B_1' \tag{A.15}$$

$$C_0' = 1.0, \alpha_o \geq B_2' \tag{A.16}$$

$$C_0' = A' - (A' - 1)\left(\frac{\alpha_o - B_1'}{B_2' - B_1'}\right), B_1' \leq \alpha_o \leq B_2' \tag{A.17}$$

the values suggested by Hasan and Kabir (1998) for A', B_1' and B_2' are shown in Table A.2.

Parameter	Value
A'	1.2
B_1'	0.4
B_1'	0.7

Table A.2: *Parameter Values for Drift Flux Calculations of Oil and Water*

Drift Velocity

For oil-in-liquid drift velocity, the suggested model is

$$V_d' = 1.53V_c'(1-\alpha_o)^2 \tag{A.18}$$

where

$$V_c' = \left(\frac{\sigma_{ow}g(\rho_w-\rho_o)}{\rho_w^2}\right)^{1/4} \tag{A.19}$$

A.3 Mixture Velocity Parameters

The velocities of the different phases can all be written as a function of mixture velocity (Eq. 3.22). Table A.3 summarizes the coefficient for each phase in terms of the calculated profile parameters and slip velocities.

Phase	Profile Parameter	Slip Velocities
Gas	C_0	V_d
Liquid	$\frac{1-\alpha_g C_0}{1-\alpha_g}$	$-\left(\frac{\alpha_g}{1-\alpha_g}\right)V_d$
Oil	$C_0'\left(\frac{1-\alpha_g C_0}{1-\alpha_g}\right)$	$V_d' - C_0'\left(\frac{\alpha_g}{1-\alpha_g}\right)V_d$
Water	$\left(\frac{1-\alpha_o C_0'}{1-\alpha_o}\right)\left(\frac{1-\alpha_g C_0}{1-\alpha_g}\right)$	$-\left(\frac{\alpha_o}{1-\alpha_o}\right)V_d' - \left(\frac{1-\alpha_o C_0'}{1-\alpha_o}\right)\left(\frac{\alpha_g}{1-\alpha_g}\right)V_d$

Table A.3: *Drift Flux Parameter Values for all Phases as a Function of Mixture Velocity*

Appendix B

Beggs and Brill (1973) Two Phase Friction Factor Correlation

The correlation holdup at a given inclination is defined as

$$H_L = H_{L(0)}\psi \tag{B.1}$$

where $H_{L(0)}$ is the equivalent liquid holdup at a horizontal angle and ψ is a correction factor. $H_{L(0)}$ is defined as

$$H_{L(0)} = \frac{a\lambda_L^b}{Fr_M^c} \tag{B.2}$$

where the coefficients a, b and c are dependent on the horizontal flow pattern. The boundaries of the different flow patterns in Figure 3.5 are described as the following:

$$L_1 = 316\lambda_L^{0.302} \tag{B.3}$$

$$L_2 = 0.0009252\lambda_L^{-2.4684} \tag{B.4}$$

$$L_3 = 0.1\lambda_L^{-1.4516} \tag{B.5}$$

$$L_4 = 0.5\lambda_L^{6.738} \tag{B.6}$$

The criteria for the flow patterns are shown in Table B.1, and the value of the coefficients a, b and c are shown in Table B.2 .

Flow Pattern	Criteria
Segregated	$\lambda_L < 0.01$ and $Fr_M^2 < L_1$, or $\lambda_L \geq 0.01$ and $Fr_M^2 < L_2$
Transition	$\lambda_L \geq 0.01$ and $L_2 \leq Fr_M^2 \leq L_3$
Intermittent	$0.01 \leq Fr_M^2 \leq 0.4$ and $L_3 \leq Fr_M^2 \leq L_1$, or $\lambda_L \geq 0.4$ and $L_3 \leq Fr_M^2 \leq L_4$
Distributed	$L_4 < 0.4$ and $Fr_M^2 \geq L_1$, or $\lambda_L \geq 0.4$ and $Fr_M^2 > L_4$

Table B.1: *Horizontal Flow Pattern Criteria*

Flow Pattern	a	b	c
Segregated	0.98	0.4846	0.0868
Transition	0.845	0.5351	0.0173
Distributed	1.065	0.5824	0.0609

Table B.2: *Parameter Values for Eq. B.2*

For 'Transitional' Flows:

$$H_{L(TRANSITION)} = A_L H_{L(SEGREGATED)} + (1 - A_L) H_{L(INTERMITTENT)} \tag{B.7}$$

$$A_L = \frac{L_3 - Fr_M^2}{L_3 - L_2} \tag{B.8}$$

The inclination correction factor, ψ is calculated via

$$\psi = 1 + C_L \Big(\sin(1.8\theta) - 0.333 \sin^3(1.8\theta) \Big) \tag{B.9}$$

$$C = (1 - \lambda_L) \ln \Big(d\prime \lambda_L^e N_{LV}^f Fr_M^g \Big) \tag{B.10}$$

where θ is the angle of the pipe from the horizontal. The coefficients d', e, f and g are listed in Table B.3.

Flow Pattern	d'	e	f	g
All Downhill	4.7	-0.3692	0.1244	-0.5056
Segregated Uphill	0.011	-3.768	3.539	-1.614
Intermittent Uphill	2.69	0.305	-0.4473	0.0978
Intermittent Uphill	$C_L = 0$ and $\psi = 1$			

Table B.3: *Parameter Values for Eq. B.10*

The dimensionless value, N_{LV} is defined as

$$N_{LV} = u_l \alpha_l \left(\frac{\rho_l}{g \sigma_{gl}} \right)^{0.25} \tag{B.11}$$

Two-Phase Friction Factor

The friction factor f for two-phase flow is calculated via Eq

$$f = \frac{1}{\left(2 \log \left(\frac{N_{Rem}}{4.5233 \log(N_{Rem}) - 3.8215} \right) \right)} e^s \tag{B.12}$$

where

$$s = \frac{\ln y}{-0.0523 + 3.128 \ln y - 0.8725 \ln^2 y + 0.01853 \ln^4 y} \tag{B.13}$$

$$y = \frac{H_L}{H_{L(0)}^2} \tag{B.14}$$

$$N_{Rem} = \frac{\rho_m u_m D}{\mu_m} \tag{B.15}$$

if $1 < y < 1.2$, then

$$s = \ln(2.2y - 1.2) \tag{B.16}$$

Appendix C

SIMPHM Further Derivations

Eqs through are substituted into Eqs 4.2,4.4 and 4.6 to form a set of linear equations as a function of the mixture velocity u_m

Water Mass

$$V_b[\rho^n(\tilde{\alpha}^{n+1}_{w,j} - \alpha^n_{w,j}) - \alpha^n_w(\tilde{\rho}^{n+1}_{w,j} - \rho^n_{w,j})] + \Delta t[\dot{\alpha}^n_{w,j+1}\dot{\rho}^n_{w,j+1}A^n_{w,j+1}(C^{ow}_{0,2}u^{n+1}_{m,j+1} + V^{ow}_{d,2}) - \dot{\alpha}^n_{w,j}\dot{\rho}^n_{w,j}A^n_{w,j}(C^{ow}_{0,2}u^{n+1}_{m,j} + V^{ow}_{d,2})] = V_b\Delta t\dot{\psi}^n_{w,j} \tag{C.1}$$

Mass Difference

$$\begin{aligned}
&V_b[\rho^n_g(\tilde{\alpha}^{n+1}_{g,j} - \alpha^n_{g,j}) - \rho^n_o(\tilde{\alpha}^{n+1}_{o,j} - \alpha^n_{o,j}) - \rho^n_w(\tilde{\alpha}^{n+1}_{w,j} - \alpha^n_{w,j})] - \\
&V_b[\alpha^n_g(\tilde{\rho}^{n+1}_{g,j} - \rho^n_{g,j}) - \alpha^n_o(\tilde{\rho}^{n+1}_{o,j} - \rho^n_{o,j}) - \alpha^n_w(\tilde{\rho}^{n+1}_{w,j} - \rho^n_{w,j})] + \\
&\Delta t[\dot{\alpha}^n_{g,j+1}\dot{\rho}^n_{g,j+1}A^n_{g,j+1}(C^{gl}_{0,1}u^{n+1}_{m,j+1} + V^{gl}_{d,1}) - \dot{\alpha}^n_{g,j}\dot{\rho}^n_{g,j}A^n_{g,j}u(C^{gl}_{0,1}u^{n+1}_{m,j} + V^{gl}_{d,1})] - \\
&\Delta t[\dot{\alpha}^n_{o,j+1}\dot{\rho}^n_{o,j+1}A^n_{o,j+1}(C^{ow}_{0,1}u^{n+1}_{m,j+1} + V^{ow}_{d,1}) - \dot{\alpha}^n_{o,j}\dot{\rho}^n_{o,j}A^n_{o,j}(C^{ow}_{0,1}u^{n+1}_{m,j} + V^{ow}_{d,1})] - \\
&\Delta t[\dot{\alpha}^n_{w,j+1}\dot{\rho}^n_{w,j+1}A^n_{w,j+1}(C^{ow}_{0,2}u^{n+1}_{m,j+1} + V^{ow}_{d,2}) - \dot{\alpha}^n_{w,j}\dot{\rho}^n_{w,j}A^n_{w,j}(C^{ow}_{0,2}u^{n+1}_{m,j} + V^{ow}_{d,2})] \\
&= V_b\Delta t(2\Gamma_g + \dot{\psi}^n_{g,j} - \dot{\psi}^n_{o,j} - \dot{\psi}^n_{w,j})
\end{aligned} \tag{C.2}$$

Mass Summation

$$
\begin{aligned}
&V_b[\rho_g^n(\tilde{\alpha}_{g,j}^{n+1}-\alpha_{g,j}^n)+\rho_o^n(\tilde{\alpha}_{o,j}^{n+1}-\alpha_{o,j}^n)+\rho_w^n(\tilde{\alpha}_{w,j}^{n+1}-\alpha_{w,j}^n)]-\\
&V_b[\alpha_g^n(\tilde{\rho}_{g,j}^{n+1}-\rho_{g,j}^n)+\alpha_o^n(\tilde{\rho}_{o,j}^{n+1}-\rho_{o,j}^n)+\alpha_w^n(\tilde{\rho}_{w,j}^{n+1}-\rho_{w,j}^n)]+\\
&\Delta t[\dot{\alpha}_{g,j+1}^n\dot{\rho}_{g,j+1}^n A_{g,j+1}^n(C_{0,1}^{gl}u_{m,j+1}^{n+1}+V_{d,1}^{gl})-\dot{\alpha}_{g,j}^n\dot{\rho}_{g,j}^n A_{g,j}^n(C_{0,1}^{gl}u_{m,j}^{n+1}+V_{d,1}^{gl})]+\\
&\Delta t[\dot{\alpha}_{o,j+1}^n\dot{\rho}_{o,j+1}^n A_{o,j+1}^n(C_{0,1}^{ow}u_{m,j+1}^{n+1}+V_{d,1}^{ow})-\dot{\alpha}_{o,j}^n\dot{\rho}_{o,j}^n A_{o,j}^n(C_{0,1}^{ow}u_{m,j}^{n+1}+V_{d,1}^{ow})]+\\
&\Delta t[\dot{\alpha}_{w,j+1}^n\dot{\rho}_{w,j+1}^n A_{w,j+1}^n(C_{0,2}^{ow}u_{m,j+1}^{n+1}+V_{d,2}^{ow})-\dot{\alpha}_{w,j}^n\dot{\rho}_{w,j}^n A_{w,j}^n(C_{0,2}^{ow}u_{m,j}^{n+1}+V_{d,2}^{ow})]\\
&=V_b\Delta t(\dot{\psi}_{g,j}^n+\dot{\psi}_{o,j}^n+\dot{\psi}_{w,j}^n)
\end{aligned}
\tag{C.3}
$$

Eqs. C.1 through C.3 are then factored and rearranged to be in the form of Eq. 4.9.

Factorized Water Mass

$$
\begin{aligned}
&[\rho^n(\tilde{\alpha}_{w,j}^{n+1}-\alpha_{w,j}^n)-\alpha_w^n(\tilde{\rho}_{w,j}^{n+1}-\rho_{w,j}^n)]=\\
&\left[\Delta t\dot{\psi}_{w,j}^n+\frac{\Delta t}{V_b}[-\dot{\alpha}_{w,j+1}^n\dot{\rho}_{w,j+1}^n A_{w,j+1}^n V_{d,2}^{ow}+\dot{\alpha}_{w,j}^n\dot{\rho}_{w,j}^n A_{w,j}^n V_{d,2}^{ow}]\right]-\\
&u_{m,j+1}^{n+1}\left[\frac{\Delta t}{V_b}\dot{\alpha}_{w,j+1}^n\dot{\rho}_{w,j+1}^n A_{w,j+1}^n C_{0,2}^{ow}\right]+u_{m,j}^{n+1}\left[\frac{\Delta t}{V_b}\dot{\alpha}_{w,j}^n\dot{\rho}_{w,j}^n A_{w,j}^n C_{0,2}^{ow}\right]
\end{aligned}
\tag{C.4}
$$

Factorized Mass Difference

$$
\begin{aligned}
&\big[\rho_g^n(\tilde{\alpha}_{g,j}^{n+1}-\alpha_{g,j}^n)-\rho_o^n(\tilde{\alpha}_{o,j}^{n+1}-\alpha_{o,j}^n)-\rho_w^n(\tilde{\alpha}_{w,j}^{n+1}-\alpha_{w,j}^n)\big]+\\
&[\alpha_g^n(\tilde{\rho}_{g,j}^{n+1}-\rho_{g,j}^n)-\alpha_o^n(\tilde{\rho}_{o,j}^{n+1}-\rho_{o,j}^n)-\alpha_w^n(\tilde{\rho}_{w,j}^{n+1}-\rho_{w,j}^n)]=\\
&\Big[\Delta t(2\Gamma_g+\dot{\psi}_{g,j}^n-\dot{\psi}_{o,j}^n-\dot{\psi}_{w,j}^n)+\Delta t\big[-\dot{\alpha}_{g,j+1}^n\dot{\rho}_{g,j+1}^n A_{j+1}^n V_{d,1}^{gl}+\dot{\alpha}_{g,j}^n\dot{\rho}_{g,j}^n A_j^n V_{d,1}^{gl}\big]+\\
&\Delta t\big[\dot{\alpha}_{o,j+1}^n\dot{\rho}_{o,j+1}^n A_{j+1}^n V_{d,1}^{ow}-\dot{\alpha}_{o,j}^n\dot{\rho}_{o,j}^n A_j^n V_{d,1}^{ow}\big]+\\
&\Delta t\big[\dot{\alpha}_{w,j+1}^n\dot{\rho}_{w,j+1}^n A_{j+1}^n V_{d,2}^{ow}-\dot{\alpha}_{w,j}^n\dot{\rho}_{w,j}^n A_j^n V_{d,2}^{ow}\big]\Big]+\\
&u_{m,j+1}^{n+1}\frac{\Delta t}{V_b}\Big[-\dot{\alpha}_{g,j+1}^n\dot{\rho}_{g,j+1}^n A_{j+1}^n C_{0,1}^{gl}+\dot{\alpha}_{o,j+1}^n\dot{\rho}_{o,j+1}^n A_{j+1}^n C_{0,1}^{ow}+\\
&\dot{\alpha}_{w,j+1}^n\dot{\rho}_{w,j+1}^n A_{j+1}^n C_{0,2}^{ow}\Big]+u_{m,j}^n\frac{\Delta t}{V_b}\Big[\dot{\alpha}_{g,j}^n\dot{\rho}_{g,j}^n A_j^n C_{0,1}^{gl}\\
&-\dot{\alpha}_{o,j}^n\dot{\rho}_{o,j}^n A_j^n C_{0,1}^{ow}-\dot{\alpha}_{w,j}^n\dot{\rho}_{w,j+1}^n A_j^n C_{0,2}^{ow}\Big]
\end{aligned}
\tag{C.5}
$$

Factorized Mass Summation

$$
\begin{aligned}
&\big[\rho_g^n(\tilde{\alpha}_{g,j}^{n+1}-\alpha_{g,j}^n)-\rho_o^n(\tilde{\alpha}_{o,j}^{n+1}-\alpha_{o,j}^n)-\rho_w^n(\tilde{\alpha}_{w,j}^{n+1}-\alpha_{w,j}^n)\big]+\\
&[\alpha_g^n(\tilde{\rho}_{g,j}^{n+1}-\rho_{g,j}^n)-\alpha_o^n(\tilde{\rho}_{o,j}^{n+1}-\rho_{o,j}^n)-\alpha_w^n(\tilde{\rho}_{w,j}^{n+1}-\rho_{w,j}^n)]=\\
&\Bigg[\Delta t(\dot{\psi}_{g,j}^n+\dot{\psi}_{o,j}^n+\dot{\psi}_{w,j}^n)+\Delta t\big[-\dot{\alpha}_{g,j+1}^n\dot{\rho}_{g,j+1}^n A_{j+1}^n V_{d,1}^{gl}+\dot{\alpha}_{g,j}^n\dot{\rho}_{g,j}^n A_j^n V_{d,1}^{gl}\big]+\\
&\Delta t\big[-\dot{\alpha}_{o,j+1}^n\dot{\rho}_{o,j+1}^n A_{j+1V_{d,1}^{ow}}^n+\dot{\alpha}_{o,j}^n\dot{\rho}_{o,j}^n A_j^n V_{d,1}^{ow}\big]+\\
&\Delta t\big[-\dot{\alpha}_{w,j+1}^n\dot{\rho}_{w,j+1}^n A_{j+1}^n V_{d,2}^{ow}+\dot{\alpha}_{w,j}^n\dot{\rho}_{w,j}^n A_j^n V_{d,2}^{ow}\big]\Bigg]+\\
&u_{m,j+1}^{n+1}\frac{\Delta t}{V_b}\Bigg[-\dot{\alpha}_{j+1}^n\dot{\rho}_{g,j+1}^n A_{g,j+1}^n C_{0,1}^{gl}-\dot{\alpha}_{o,j+1}^n\dot{\rho}_{o,j+1}^n A_{j+1}^n C_{0,1}^{ow}-\\
&\dot{\alpha}_{w,j+1}^n\dot{\rho}_{w,j+1}^n A_{j+1}^n C_{0,2}^{ow}\Bigg]+u_{m,j}^n\frac{\Delta t}{V_b}\Bigg[\dot{\alpha}_{g,j}^n\dot{\rho}_{g,j}^n A_j^n C_{0,1}^{gl}-\\
&\dot{\alpha}_{o,j}^n\dot{\rho}_{o,j}^n A_j^n C_{0,1}^{ow}-\dot{\alpha}_{w,j}^n\dot{\rho}_{w,j+1}^n A_j^n C_{0,2}^{ow}\Bigg]
\end{aligned}
\tag{C.6}
$$

hence, the transport equations are factorized in terms of the primary variables $\Delta\tilde{\alpha}_w, \Delta\tilde{\alpha}_g, \Delta P, u_{m,j+1}^{n+1}$ and $u_{m,j}^{n+1}$. The factors of these terms make up the entries of $A(I,1), A(I,2), A(I,3), B(I), M_1(I)$ and $M_0(I)$ in Eq 4.9. Likewise, Eq. 4.8 is factorized to be in terms of $u_{m,j}^{n+1}$ and ΔP:

Factorized Momentum Conservation

$$
\begin{aligned}
&u_{m,j}^{n+1}\Bigg[\Delta t\rho_{m,j}^{n+1}+\Delta t\Delta x\frac{1}{2}\frac{\rho_{m,j}^n|u_{m,j}^n|}{D}+\Delta t\Delta x(\dot{\psi}_{g,j}^n+\dot{\psi}_{o,j}^n+\dot{\psi}_{w,j}^n)\Bigg]=(P_j^{n+1}-P_{j-1}^{n+1})[-\Delta t144g_c]+\\
&\Bigg[\Delta x\rho_m^n u_{m,j}^n-\frac{1}{2}\Delta t\rho_{m,j}^n\big((u_{m,L}^n)^2-(u_{m,K}^n)^2\big)-\Delta t\Delta x\rho_{m,j}^n g_c\sin\theta\Bigg]
\end{aligned}
\tag{C.7}
$$

the factorized terms of Eq. C.7 represent the entries of $X(I), Y(I)$ and $Z(I)$ respectively.

Bibliography

Ambrus, A., Aarsnes, U. J. F., Vajargah, A. K., Akbari, B., and Oort, E. van, "A Simplified Transient Multi-Phase Model for Automated Well Control Applications", IPTC-18481-MS, Presented at International Petroleum Technology Conference, Doha, Qatar, Dec. 2015.

Avelar, C. S., Ribeiro, P., and Sepehrnoori, K., "Deepwater Gas Kick Simulation", *Journal of Petroleum Science and Engineering* 67.1–2 (2009), pp. 13–22.

Avelar, C. S., "Modelagem do Controle de Pocos por Diferencas Finitas (Well Control Modelling by Finite Differences)", Portuguese, Master's Thesis, Universidade Estadual de Campinas, 2008.

Aziz, K., Govier, G. W., and Fogarrasi, M., "Pressure Drop in Wells Producing Oil and Gas", *Journal of Canadian Petroleum Technology* 3.12 (July 1972), pp. 38–48.

Beggs, H. and Brill, J., "A Study of Two Phase Flow in Inclined Pipes", *Journal of Petroleum Technology* 25.5 (Apr. 1973), pp. 607–109.

Beggs, H. and Robinson, J., "Estimating the Viscosity of Crude Oil Systems", *Journal of Petroleum Technology* 29.09 (Sept. 1975), pp. 1140–1141.

Bourgoyne Jr, A., Chenevert, M. T., Millheim, K. K., and Young Jr, F., *Applied Drilling Engineering*, Society of Petroleum Engineers, 1985.

Costa, S., Da Fontoura, S., and Martins, A., "Simulation of Transient Cuttings Transportation and ECD in Wellbore Drilling", SPE-113893-MS, Presented at SPE Europec/EAGE Annual Conference and Exhibition, Rome, Italy, June 2008.

De Ghetto, G., Paone, F., and Villa, M., "Pressure-Volume-Temperature Correlations for Heavy and Extra Heavy Oils", SPE-30316-MS, Presented at SPE International Heavy Oil Symposium, Calgary, Alberta, Canada, June 1995.

Dranchuk, P. and Abou-Kassem, H., "Calculation of Z Factors For Natural Gases Using Equations of State", *Journal of Canadian Petroleum Technology* 14.3 (July 1975).

Falk, K., Fossli, B., Lagerberg, C., and others., "Well Control When Drilling With a Partly-Evacuated Marine Drilling Riser", SPE-143095-MS, Denver, Colorado, USA, Apr. 2011.

Fjelde, K. K. and Karlsen, K. H., "High-Resolution Hybrid Primitive Conservative Upwind Schemes for the Drift Flux Model", *Computers and Fluids* 31.3 (2002), pp. 335–367.

Fossli, B. and Sangesland, S., "Managed Pressure Drilling for Subsea Applications: Well Control Challenges in Deep Waters", SPE-91633-MS, Presented at SPE/IADC Underbalanced Technology Conference and Exhibition, Houston, Texas, Oct. 2004.

Hagendorn, A. and Brown, K., "Experimental Study of Pressure Gradients Ocurring During Continuous Two Phase Flow in Small Diameter Vertical Conduits", *Journal Petroleum Technology* 14.4 (1965), pp. 475–485.

Hall, K. and Yarborough, L., "A New Equation of State for Z-Factor Calculations.", *Oil and Gas Journal* 71.25 (1973).

Hasan, A. and Kabir, C., "A Simplified Model for Oil-Water Flow in Vertical and Deviated Wellbores", SPE-49163-MS, Presented at SPE Annual Technical Conference and Exhibition, New Orleans, Louisiana, USA, Sept. 1998.

Hibiki, T. and Ishii, M., "One-Dimensional Drift-flux Model and Constitutive Equations for Relative Motion between Phases in Various Two-Phase Regimes", *International Journal of Heat and Mass Transfer* 46 (2003), pp. 4935–4948.

Kaya, A., Sarica, C., and Brill, J., "Comprehensive Mechanistic Modeling of Two-Phase Flow in Deviated Wells", SPE-56522-MS, Presented at Annual Technical Conference and Exhibition, Houston, Texas, Oct. 1999.

Leblanc, J. and Lewis, R., "A Mathematical Model of a Gas Kick", *Transanctions* 243 (1968), pp. 888–898.

Lee, A., Gonzalez, M., and Eakin, B., "The Viscosity of Natural Gases", *Journal of Canadian Petroleum Technology* 18.8 (1966), pp. 997–1000.

Loiola, C. H. d. O., "Simulacao Composicional De Controle De Pocos (Compositional Well Control Simulation)", Portuguese, Master's Thesis, Universidade Estadual de Campinas, Sept. 2015.

Marques, M., "Desenvolvimento e Validacao Experimental de Procedimentos de Controle de Poco em Situacoes Especiais (Development and Experimental Validation Well Control Procedures in Special Situations)", Portuguese, Master's Thesis, UFRJ: Universidade Federal do Rio de Janeiro, 2004.

McCain, W. D., *Properties of Petroleum Fluids*, Tulsa, OK: Penwell Publishing Company, 1989.

Mehrabi, M., Zeyghami, M., and Shahri, M., "Modeling of Fracture Ballooning in Naturally Fractured Reservoirs: A Sensitivity Analysis", SPE 163034, Presented at Nigeria Annual International Conference and Exhibition, Abuja, Nigeria, Aug. 2012.

Mishima, K. and Ishii, M., "Flow Regime Transition Criteria for Upward Two-Phase Flow in Vertical Tubes", vol. 27, 5, May 1984, pp. 723–737.

Nickens, H. V., "A Dynamic Computer Model of a Kicking Well: Part ll -Model Predictions and Conclusions", *SPE Drilling Engineering* (June 1987), pp. 159–173.

Nunes, J., Bannwart, A., and Ribeiro, P., "Mathematical Modeling of Gas Kicks in Deep Water Scenario.", SPE-77253-MS, Presented at IADC/SPE Asia Pacific Drilling Technology, Jakarta, Indonesia, Sept. 2002.

Orkiszewski, J., "Predicting Two-Phase Pressure Drops in Vertical Pipe", *Journal Petroleum Technology* 19.6 (June 1967), pp. 829–838.

Pourafshary, P., "A Coupled Wellbore/Reservoir Simulator To Model Multiphase Flow and Temperature Distribution", Doctoral Dissertation, The University of Texas at Austin, 2007.

Rader, D., Bourgoyne Jr, A., and Ward, R., "Factors Affecting Bubble-Rise Velocity Of Gas Kicks", *Journal of Petroleum Technology* 27.5 (May 1975), pp. 571–584.

Rommetveit, R. and Vefring, E. H., "Comparison of Results From an Advanced Gas Kick Simulator With Surface and Downhole Data From Full Scale Gas Kick Experiments in an Inclined Well", SPE 22558, Presented at SPE Annual Technical Conference and Exhibition, Dallas, Texas, Oct. 1991.

Santos, O., "Well-Control Operations in Horizontal Wells", *SPE Drilling Engineering* (June 1991), pp. 111–117.

Shahri, M. P. and Mehrabi, M., "A New Approach in Modeling of Fracture Ballooning in Naturally Fractured Reservoirs", SPE 163382, Presented at SPE Kuwait International Petroleum Conference and Exhibition, Kuwait City, Kuwait, Dec. 2012.

Shi, H., Holmes, J. A., Durlofsky, L. J., Aziz, K., Diaz, L., Alkaya, B., and Oddie, G., "Drift-Flux Modeling of Two-Phase Flow in Wellbores", *SPE Drilling and Completion* 10 (Mar. 2005), pp. 24–33.

Shirdel, M., "Development of a Coupled Wellbore/Reservoir Simulator for Damage Prediction and Remediation", Doctoral Dissertation, The University of Texas at Austin, 2013.

Shirdel, M. and Sepehrnoori, K., "Development of Transient Mechanistic Three-Phase Flow Model for Wellbores", *SPE Journal* 22.01 (Feb. 2017), pp. 374–388.

Shoham, O., *Mechanistic Modelling of Gas-Liquid Two Phase Flows in Pipes*, University of Tulsa: Society of Petroleum Engineers, 2005.

Standing, M., *Volumetric and Phase Behaviour of Oil Field Hydrocarbon Systems*, Dallas, TX: Society of Petroleum Engineer, 1977.

Starrett, M. P., Hill, A. D., and Sepehrnoori, K., "A Shallow-Gas-Kick Simulator Including Diverter Performance", *SPE Drilling Engineering* (Mar. 1990), pp. 79–85.

Taitel, Y. and Dukler, A., "Modelling Flow Pattern Transition for Steady Upward Gas-Liquid Flow in Vertical Tubes", *AIChE Journal* 26.3 (May 1980), pp. 345–354.

Udegbunam, J. E., Fjelde, K. K., Evje, S., and Nygaard, G., "On the Advection Upstream Splitting Method Hybrid Scheme: A Simple Transient-Flow Model for Managed Pressure Drilling and Underbalanced Drilling Applications", *SPE Drilling and Completion* 30.2 (2015), pp. 98–109.

Vasquez, M. and Beggs, H., "Correlations for Fluid Physical Property Predictions", *Journal of Petroleum Technology* 32.6 (June 1980), pp. 968–970.

White, F. M., *Fluid Mechanics, Sevent Edition*, University of Rhode Island: (Mcgraw-Hill Series in Mechanical Engineering), 2010.

Yuan, M. and Zhou, D., "Evaluation of Two-phase Flow Correlation and Mechanistic Models for Pipelines at Horizontal and Inclined Upward Flow", SPE-120281-MS, Presented at SPE Production and Operation Symposium, Oklahoma City, Oklahoma, Apr. 2009.